*J. Fluid Mech.* (2009), *vol.* 623, *pp.* 241–271.  
doi:10.1017/S0022112008005284 Printed in the United Kingdom

# Destabilizing effects of confinement on homogeneous mixing layers

J. J. HEALEY†

Department of Mathematics, Keele University, Keele, Staffs ST5 5BG, UK

(Received 30 July 2008 and in revised form 6 November 2008)

The absolute and convective instability properties of plane mixing layers are investigated for linearized inviscid disturbances. It is shown that confinement by plates parallel to the flow can enhance the absolute instability so much that even a co-flow plane mixing layer becomes absolutely unstable when the ratio of distances of the plates from the mixing layer lies in a certain range. Even when the plates are placed equidistantly from the mixing layer, a co-flow mixing layer can become absolutely unstable if the velocity profile has an asymmetry about its mid-plane. 'Semiconfinement', where a plate is only added to one side of the mixing layer, is also investigated. A substantial destabilization is possible when the plate is added on the side of the faster stream. Previous investigations seem only to have found absolute instability when the streams flow in opposite directions.

## 1. Introduction

A flow is called absolutely unstable if growing disturbances propagate both upstream and downstream of the disturbance source, and convectively unstable if they only grow as they propagate away from the source. This distinction can have important physical consequences because an absolute instability can generate a global mode with an intrinsic natural frequency that dominates the flow, while convectively unstable flows amplify certain extrinsic disturbances as they are carried downstream. These ideas, and a method for distinguishing between absolute and convective instabilities, were developed in the early 1960s in the field of plasma physics (see Briggs 1964), and independently by Gaster (1968) in hydrodynamics. However, they started to have a major impact in hydrodynamic stability theory following Huerre & Monkewitz (1985)'s application of Briggs' method to an inviscid plane mixing layer, and here we return to this classic problem.

We consider plane mixing layers whose streams have constant dimensional velocities $U_1^*$ and $U_2^*$ far from the mixing layer. In particular, making velocities dimensionless using $(U_1^* + U_2^*)/2$, we examine mixing layers written in the form

$$U(y) = 1 + rf(y), \tag{1.1}$$

where $U$ is the dimensionless basic flow in the $x$ direction, $y$ is in the cross-stream direction, $\lim_{y\to\pm\infty} f(y) = \pm 1$ and $r = (U_1^* - U_2^*)/(U_1^* + U_2^*)$. Lengths have been scaled on some convenient measure of shear-layer thickness. Without loss of generality, we shall consider $r > 0$. We refer to the case $r < 1$ as a co-flow mixing layer since $U_1^*$ and $U_2^*$ then have the same sign, and the case $r > 1$, where $U_1^*$ and $U_2^*$ have opposite

† Email address for correspondence: j.j.healey@maths.keele.ac.uk

signs, as a counter-flow mixing layer. Intuitively, one expects the mixing layer to be convectively unstable when $r$ is small enough, and absolutely unstable when $r$ is large enough. Huerre & Monkewitz used $f(y) = \tanh(y/2)$ and found that the transition from convective to absolute instability occurs at $r = r_t = 1.315$, i.e. when the counter-flow is sufficiently strong.

Huerre & Monkewitz also noted a difficulty in the application of Briggs' method that arises when $r < 0.84$. In Briggs' method the solution to the initial-value problem posed by introducing an impulsive disturbance to an otherwise undisturbed flow is expressed as an inverse Fourier–Laplace transform. The integration paths are placed according to the principles of causality and residue theory is used to evaluate the $\omega$ (angular frequency) integral, leaving an integral over $\alpha$ (streamwise wavenumber). At large times this integral may be estimated asymptotically by deforming the integration path through certain saddle points in the complex $\alpha$ plane where $\mathrm{d}\omega/\mathrm{d}\alpha = 0$. The dominant saddle, called the 'pinch point' in Briggs' terminology, is found by mapping out contours of constant $\mathrm{Im}(\omega)$ in the complex $\alpha$ plane. Essentially, the pinch point is the highest saddle point whose valleys contain the real $\alpha$ axis as $\alpha \to \pm\infty$.

When $r < 0.84$, the pinch point moves into the $\mathrm{Re}(\alpha) < 0$ half-plane, i.e. the left half-plane. Such waves appear unphysical because modes continued into the left half-plane grow exponentially with distance from the shear layer, and so fail to satisfy homogeneous boundary conditions. This can be seen by considering the Rayleigh equation, which describes small amplitude disturbances in the form $v(y)\exp \mathrm{i}(\alpha x - \omega t)$ superimposed on a basic flow $U(y)$,

$$(U - c)(v'' - \alpha^2 v) - U''v = 0, \tag{1.2}$$

where $v$ is the vertical component of the disturbance velocity and $c = \omega/\alpha$. The boundary conditions for mixing layers are $v \to 0$ as $y \to \pm\infty$, which defines an eigenvalue problem, whose solution gives the dispersion relation, i.e. a relationship between $\alpha$ and $\omega$ see Drazin & Reid (1981). When $y \to \infty$, $U \to 1 + r$ by (1.1), so (1.2) reduces to

$$v'' - \alpha^2 v = 0, \tag{1.3}$$

provided $c \neq 1 + r$. The solution to (1.3) satisfying homogeneous boundary conditions is $v = A\exp(-\alpha y)$ when $\mathrm{Re}(\alpha) > 0$, where $A$ is an arbitrary constant. If a solution of the dispersion relation is followed across the imaginary $\alpha$ axis from the right half-plane into the left half-plane, then $v$ would increase exponentially in $y$, and no longer satisfy homogeneous boundary conditions. Similar considerations apply as $y \to -\infty$. This is the difficulty encountered by Huerre & Monkewitz; for $r < 0.84$ their shear layer has no pinch point satisfying homogeneous boundary conditions. However, at these values of $r$, $\mathrm{Im}(\omega) < 0$ at the pinch point, i.e. disturbances decay exponentially in time, and this case was not studied further.

In fact, left half-plane modes have been observed in a number of different flows: in swirling jets (see Lim & Redekopp 1998), and in plane and circular jets and wakes of various density ratios (see Yu & Monkewitz 1990; Juniper & Candel 2003; Juniper 2006), but in these studies they were dismissed as non-physical.

Nonetheless, left half-plane modes do have a physical interpretation, and furthermore, as we discuss below, they can imply that confinement of such a flow in the cross-stream direction can strengthen or even create absolute instability. Therefore, Huerre & Monkewitz's observation of left half-plane modes in the mixing layer suggests that this flow may also be destabilized by confinement. In the present work,

we investigate this possibility and show that the effect can be sufficiently strong that even co-flow mixing layers can become absolutely unstable.

Understanding left half-plane modes follows from remembering that one is interested in an initial-value problem in which initially the flow is undisturbed. After the disturbance has been introduced, the flow remains undisturbed far from the disturbance source due to the finite propagation velocities of the disturbance. Therefore, homogeneous boundary conditions are always satisfied. If a disturbance with the frequency of an unstable left half-plane mode is introduced, then it propagates in the $y$ direction, growing exponentially in $y$ behind a front, beyond which the flow is undisturbed, and homogeneous boundary conditions are satisfied. This, perhaps surprising, scenario was discovered by Healey (2006*b*) in a study of disturbances in the rotating-disk boundary layer, where it had been found that the pinch point for this flow can become asymptotically close to the imaginary $\alpha$ axis, giving rise to unstable left half-plane modes (see Healey 2006*a*). It was shown that asymptotic saddle point calculations, based on left half-plane modes, for propagation velocities, and exponential growth rates in $y$, agree with numerical evaluation of the inverse transforms where the integration path is made up of the usual right half-plane modes. It was also shown how disturbance energy generated inside the boundary layer in the main part of the disturbance is carried outside the boundary layer and back upstream in such a way that sustains this wall-normal growth in a region of zero-mean shear, and therefore zero-Reynolds stress. These papers show that the left half-plane modes have the character of a convective instability in the crossflow direction.

Waves that grow in the cross-stream direction turn out to be very sensitive to the boundary condition applied far from the shear layer. In an unconfined inviscid shear layer the outer boundary condition is of exponential decay, i.e. $v'(y) = -\alpha v(y)$ at some large value of $y$, but in an inviscid shear layer confined by a plate at $y = h$ the outer boundary condition is zero normal-flow at the plate, i.e. $v(h) = 0$. When $h \gg 1$ the usual right half-plane modes are little affected by confinement because the modes of the unconfined flow are exponentially small at $y = h$, so confinement produces only a small modification to the dispersion relation, and in fact typically stabilizes temporal waves (see § 2). However, flows with unstable left half-plane modes are controlled by the properties of the dispersion relation near the imaginary $\alpha$ axis, i.e. by the continuous spectrum associated with the branch cut of the square-root in the solution outside a shear layer when it is written in the form $v = A \exp(-\sqrt{\alpha^2} y)$ for $y$ large and positive (this form makes it clear that it is the decaying solution of (1.3) that is to be taken, regardless of the sign of $\mathrm{Re}(\alpha)$). Following a mode into the left half-plane requires deforming this branch cut from the imaginary $\alpha$ axis. The dispersion relation near the imaginary $\alpha$ axis is strongly affected by confinement when $\mathrm{Re}(\alpha) = O(h^{-1})$, i.e. when wavelengths are comparable to the distance to the confining plate. Confinement causes the branch cut to be replaced by an infinite discrete spectrum, which leads to infinitely many new saddle points lying close to the imaginary $\alpha$ axis, some of which dominate the pinch point of the unconfined problem, as shown by Healey (2007). Confinement therefore creates a new pinch point, which destabilizes or can create absolute instability in flows with unstable left half-plane modes.

Juniper (2007) used these ideas to extend his earlier work, Juniper (2006), in which the left half-plane modes were excluded, so as to reinstate these modes in the jet/wake problem. Juniper (2007) also considered the effect of finite thickness shear layers at the jet/wake edge, but concluded that they only affect the growth in frames of reference moving downstream, and so could be ignored when determining criteria for

absolute instability. In the present paper, we identify circumstances where the detail of the mixing-layer profile cannot be ignored in determining criteria for absolute instability.

However, it seems that the first paper to recognize that confinement creates a family of saddle points near the imaginary wavenumber axis was Koch (1985) in an early application of Briggs' method to a hydrodynamic stability problem. He studied the inviscid compressible spatio-temporal stability of families of confined wake profiles, including the piecewise-linear model considered by Juniper (2006). Koch's primary interest was in the saddle points of the unconfined version of the problem, but his computational technique required a finite cross-stream domain, leading to the appearance of the family of confinement saddle points. In his § 4.1, Koch notes that a confinement saddle point can sometimes dominate the problem, and although he questions its physical relevance, he points out that this shows the importance that sidewalls, i.e. confinement, can have in spatio-temporal problems. We can now recognize this as perhaps the earliest observation of destabilization of an absolute instability by confinement.

When the left half-plane modes are unstable, the destabilizing effect of confinement persists even as $h \to \infty$. However, Huerre & Monkewitz showed that the left half-plane modes are stable for the mixing layer. Nonetheless, we shall show that symmetric confinement (plates equidistant from the mixing layer) is destabilizing for a finite range of $h$ (see § 3). Furthermore, we show that a much stronger destabilization can occur when the shear layer is asymmetrically confined, i.e. when the two plates are at different distances from the mixing layer (see § 4). This effect persists even as plate separation tends to infinity, and is independent of the velocity profile in the mixing layer. This large-separation limit, where the plates are far apart compared with the mixing-layer thickness, corresponds to the case of varicose modes of the confined jet/wake profile studied by Juniper (2006). However, with symmetric confinement the absolute instability is always sensitive to the form of the velocity profile. In § 5 we identify a class of velocity profiles that are particularly absolutely unstable under symmetric confinement. What we call 'semiconfinement', where a plate is only added to one side of the mixing layer, is studied in § 6. Even though the continuous spectrum is not replaced by an infinite discrete spectrum, substantial destabilization is still found, and the effect persists when the plate is arbitrarily far from the mixing layer, and again occurs regardless of the details of the mixing-layer profile. In this limit where the plate is far from the mixing layer, we again recover a case considered by Juniper (2006), and also by Yu & Monkewitz (1990), that of varicose modes of an unconfined jet/wake profile. Conclusions are drawn in § 7.

## 2. Temporal instability of confined mixing layers

Rayleigh (1894) showed that confining an inviscid piecewise-linear mixing layer by placing plates at $y = \pm h$, and imposing boundary conditions $v(\pm h) = 0$, i.e. symmetric confinement, has a stabilizing effect, which becomes more pronounced when the flow is more strongly confined, i.e. as $h$ is reduced, and a sufficiently strong confinement completely stabilizes the flow to inviscid disturbances (see § 23 of Drazin & Reid 1981).

This conclusion remains true for smooth velocity profiles, and in this section we derive some general results for the confinement of arbitrary profiles (1.1) with the property $f(-y) = -f(y)$. The qualitative effects of asymmetric confinement by plates

at $y = h_1$, $y = -h_2$, $h_1 \neq h_2$, and semiconfinement by a single plate on just one side of the mixing layer are compared with the case of symmetric confinement.

Our theoretical results concern the neutral curve as confinement parameters are varied. The effect of confinement on growth rates will be illustrated using numerical solutions of the Rayleigh equation. Neutral waves have a critical point, $y_c$, where $U(y_c) = c$, that coincides with the inflexion point where $U'' = 0$. When $f(-y) = -f(y)$ this implies $y_c = 0$, and therefore $c = 1$, thus reducing (1.2) to

$$f(v'' - \alpha^2 v) - f'' v = 0. \tag{2.1}$$

This equation, with appropriate homogeneous boundary conditions, gives an eigenvalue problem for $\alpha$ on the neutral curve. The neutral curve for temporal instability is therefore independent of $r$, but the growth rates of unstable waves do depend on $r$. Further results can be obtained in the long-wave limit, i.e. when $\alpha$ is small (see § 2.1), and they will be illustrated using a tanh mixing-layer profile in § 2.2, for which further analytical results can be obtained.

### 2.1. *Effects of confinement on temporal stability in the long-wave limit*

The intercept of the neutral curve with the $\alpha = 0$ axis can be obtained by noting that when $\alpha = 0$, $v = f$ is a solution to (2.1). The second independent solution can be found by making the substitution $v(y) = f(y)V(y)$ in (2.1), and then the solution satisfying $v(-h_2) = 0$ can be written as

$$v = f(y)\left[\int_{-h_2}^{y} \frac{1}{f(t)^2} - \frac{1}{f'(0)^2 t^2}\,\mathrm{d}t - \frac{1}{f'(0)^2}\left(\frac{1}{y} + \frac{1}{h_2}\right)\right]. \tag{2.2}$$

The case of asymmetric confinement is obtained by applying the homogeneous boundary condition, $v(h_1) = 0$, to (2.2) to give the eigenrelation

$$0 = \int_{-h_2}^{h_1} \frac{1}{f(t)^2} - \frac{1}{f'(0)^2 t^2}\,\mathrm{d}t - \frac{h_1 + h_2}{h_1 h_2 f'(0)^2}. \tag{2.3}$$

For example, if $h_2$ is specified, then $h_1$ given by solving (2.3) gives the point where the neutral curve meets the $\alpha = 0$ axis. There are unstable waves when $h_1$ is greater than this critical value, and only stable waves when $h_1$ is less than this value.

We now show that the case of symmetric confinement, $h_1 = h_2 = h_s$, is a local minimum of the plate separation $h_1 + h_2$ for neutral waves as $\alpha \to 0$. This means that for a given plate separation with $h_1 + h_2 > 2h_s$, where $h_s$ is the root of

$$0 = \int_{-h_s}^{h_s} \frac{1}{f(t)^2} - \frac{1}{f'(0)^2 t^2}\,\mathrm{d}t - \frac{2}{h_s f'(0)^2}, \tag{2.4}$$

the most unstable configuration (locally) is when the mixing layer is exactly halfway between the plates. Consider $h_2$ close to $h_s$, and then solve (2.3) for $h_1$ for neutral waves, i.e. let

$$h_2 = h_s + \delta, \tag{2.5a}$$

$$h_1 = h_s + h_{11}\delta + h_{12}\delta^2 + \cdots, \tag{2.5b}$$

where $|\delta| \ll 1$. Substituting (2.5) into (2.3), equating like powers of $\delta$, and solving for $h_{11}$ and $h_{12}$, gives

$$h_1 = h_s - \delta + \frac{2f'(h_s)}{f(h_s)}\delta^2 + \cdots \tag{2.6}$$

(see Appendix A for details).

The plate separation for neutral waves for slightly asymmetric confinement, $h_1 + h_2 = 2h_s + 2f'(h_s)/f(h_s)\delta^2$, is therefore larger than the plate separation for neutral waves for symmetric confinement, $2h_s$, provided $f$ increases monotonically with $y$. Note, however, that if $f$ is not monotonic, e.g. if the basic velocity in the mixing layer overshoots its value in the free stream, causing $f'(h_s) < 0$, then the most confined flow that can support unstable waves will be asymmetrically confined, and not symmetrically confined.

The case of semiconfinement by a single plate is not directly obtained simply by letting $h_1 \to \infty$ in (2.3) because the integral is then not convergent. Instead, we write the solution (2.2) in the form

$$v = f(y)\left[\int_{-h_2}^{y} \frac{1}{f(t)^2} - \frac{1}{f'(0)^2 t^2} - 1 \, \mathrm{d}t + y + h_2 - \frac{1}{f'(0)^2}\left(\frac{1}{y} + \frac{1}{h_2}\right)\right]. \tag{2.7}$$

As $y \to \infty$ we require $v \propto \exp(-\alpha y)$, which can be seen by letting $f \to 1$ in (2.1). The solution (2.7) is only valid for small $\alpha$, and so the required behaviour of (2.7) as $y$ increases is that it should become proportional to $1 - \alpha y$, the first two terms in the Taylor expansion for $\exp(-\alpha y)$. Therefore,

$$\alpha \sim -\left[\int_{-h_2}^{\infty} \frac{1}{f(t)^2} - \frac{1}{f'(0)^2 t^2} - 1 \, \mathrm{d}t + h_2 - \frac{1}{f'(0)^2 h_2}\right]^{-1}. \tag{2.8}$$

This expression is only valid when the right-hand side of (2.8) is small, which happens when $h_2$ is small, and in this limit we obtain an expression for the neutral curve for semiconfinement when the plate at $y = -h_2$ is close to the centre of the mixing layer,

$$\alpha \sim f'(0)^2 h_2. \tag{2.9}$$

The same result is obtained when the mixing layer is confined at $y > 0$, since this corresponds to replacing $f$ by $-f$.

### 2.2. *Effects of confinement on the temporal stability of a* tanh *mixing-layer profile*

Here we illustrate the results obtained in § 2.1 using

$$f(y) = \tanh(y/2), \tag{2.10}$$

which is to be substituted into (2.1), and gives the mixing-layer profile (1.1). Although (2.10) does not typically arise as a solution to the Navier–Stokes equation, or to boundary-layer equations, it is a convenient model mixing layer for which some exact analytical stability results can be derived. Furthermore, it is the profile used by Huerre & Monkewitz (1985) in their study of the absolute instability of an unconfined mixing layer. We shall also use this model profile to illustrate the effects of confinement on absolute instability in subsequent sections of the present paper.

It may be verified that the general solution of (2.1), when $f$ is given by (2.10), is

$$v = A_1\left[2\alpha\cosh(\alpha y) - \sinh(\alpha y)\tanh\left(\frac{y}{2}\right)\right] + A_2\left[2\alpha\sinh(\alpha y) - \cosh(\alpha y)\tanh\left(\frac{y}{2}\right)\right], \tag{2.11}$$

where $A_1$ and $A_2$ are arbitrary constants (see Michalke 1964).

The only eigenvalue for the unconfined case, where $\lim_{y\to\pm\infty} v = 0$, is $\alpha = 1/2$, and the eigenfunction is given by $A_2 = 0$, i.e. $v = A_1 \mathrm{sech}(y/2)$. The unconfined flow is unstable for $0 < \alpha < 1/2$, and stable for $\alpha > 1/2$. We shall show that the neutral

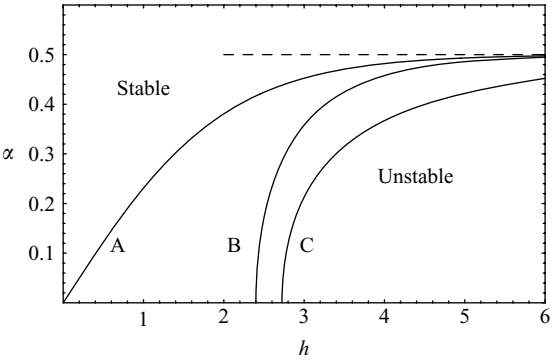


FIGURE 1. Dashed line is neutral wavenumber for temporal instability of the unconfined mixing layer (2.10), $\alpha = 1/2$. Solid lines are neutral curves for temporal instability of the same mixing layer subject to confinement: A is for semiconfinement by a single plate placed at $y = h$, (2.12); B is for symmetric confinement by plates placed at $y = \pm h$, (2.13); C is for asymmetric confinement by plates at $y = h_1$ and $y = -h_2$ where $h_2 = 3h_1$ and $h$ is half the width of the channel, $h = (h_1 + h_2)/2$, (2.14).

curves for temporal stability for confined flow all asymptote towards $\alpha = 1/2$ as the plates are moved away from the mixing layer. In fact, they approach this asymptote exponentially fast.

The neutral curve for temporal stability in the semiconfined case, with boundary conditions $v(-h) = \lim_{y \to \infty} v = 0$, is obtained using $A_2 = -A_1$, so that $v \propto \exp(-\alpha y)$ as $y \to \infty$. Applying the boundary condition $v(-h) = 0$ gives the following equation for the neutral curve for temporal instability of a semiconfined mixing layer:

$$\alpha = \frac{1}{2} \tanh\left(\frac{h}{2}\right). \tag{2.12}$$

The same equation is obtained when the plate is placed on the other side of the mixing layer. For small $h$, (2.12) reduces to (2.9), and for large $h$, $\alpha \to 1/2$ from below.

The neutral curve for temporal stability in the symmetrically confined case, with boundary conditions $v(\pm h) = 0$, is obtained from taking $A_2 = 0$, to give an even eigenfunction, and points on the neutral curve then satisfy

$$0 = 2\alpha - \tanh(\alpha h) \tanh\left(\frac{h}{2}\right). \tag{2.13}$$

As $\alpha \to 0$, (2.13) reduces to $0 = 2 - h \tanh(h/2)$, in agreement with (2.4), and it has root $h \approx 2.399$. Developing a large-$h$ asymptotic approximation to (2.13), we find $\alpha \sim (1/2) \tanh^2(h/2)$, which approaches $\alpha = 1/2$ more slowly than (2.12).

The neutral curve for symmetric confinement, (2.13), therefore lies below, and to the right, of the neutral curve for semiconfinement, (2.12), i.e. symmetric confinement is more stable than semiconfinement (see figure 1).

The results in § 2.1 indicate that for a given plate separation, $h_1 + h_2$, asymmetric confinement is more stable than symmetric confinement, and this can also be illustrated for the mixing layer (2.10). The equation for the neutral curve for asymmetric confinement is found by eliminating $A_1$ and $A_2$ from the pair of simultaneous equations obtained by setting $v(h_1) = 0$ and $v(-h_2) = 0$ in (2.11)

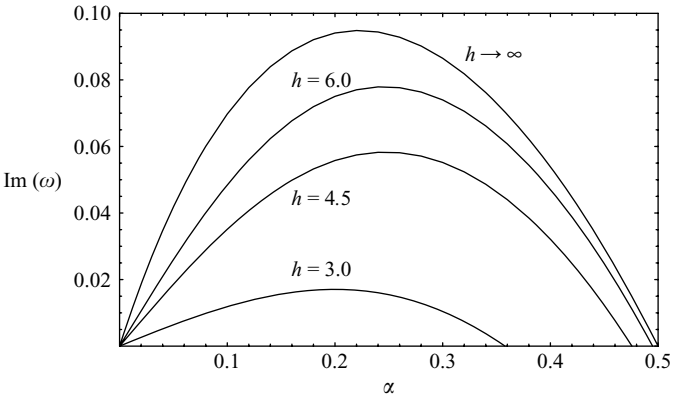


FIGURE 2. Growth rates for temporal instability of the mixing layer (2.10) substituted into (1.2) confined by plates at $y = \pm h$ and with shear strength $r = 1$. The curve labelled $h \to \infty$ corresponds to the unconfined flow.

to give

$$0 = \frac{2\alpha \tanh(\alpha h_1) - \tanh(h_1/2)}{2\alpha - \tanh(\alpha h_1)\tanh(h_1/2)} + \frac{2\alpha \tanh(\alpha h_2) - \tanh(h_2/2)}{2\alpha - \tanh(\alpha h_2)\tanh(h_2/2)}. \tag{2.14}$$

If we let $h_2 = \theta h_1$, with $\theta > 1$, then for large plate separations the neutral curve behaves like $\alpha \sim (1/2)\tanh(h_1/2)$, which approaches the unconfined limit, $\alpha = 1/2$, more slowly than the case of symmetric confinement with the same plate separation, because $2h = h_1 + h_2 \Rightarrow h_1 = 2h/(1+\theta) < h$. Therefore, the neutral curve for asymmetric confinement by plates a certain distance apart lies to the right, and below, the neutral curve for symmetric confinement.

Examples of neutral curves for semiconfinement, symmetric confinement and asymmetric confinement are given in figure 1, which confirms the progressively increasing stabilization of these three cases, respectively.

Although figure 1 shows that confinement does not affect much the neutral curve for temporal instability for symmetric confinement for $h \geqslant 6$, it has a relatively strong stabilizing effect on the growth rate at $h = 6$, and for smaller $h$, especially for the longer waves (see figure 2). These growth rates require a numerical solution of (1.2), and depend on the shear strength, $r$.

## 3. Absolute instability of a symmetrically confined mixing layer

Despite the clear stabilizing effect of confinement on the temporal instability of the mixing layer, confinement can destabilize an absolute instability, and Huerre & Monkewitz's observation that the pinch point can enter the left half of the complex wavenumber plane indicates that this could be the case for the mixing layer. The reasoning behind this unexpected assertion follows from the singular nature of the perturbation on the dispersion relation produced by weak confinement (i.e. when $h$ is large). The solution to (1.3), $v \propto \exp(-\alpha y)$, confirms that confinement has a negligible effect on the dispersion relation when $\mathrm{Re}(\alpha)h \gg 1$, and also tells us that confinement has a significant effect when $\mathrm{Re}(\alpha) = O(h^{-1})$, i.e. close enough to the imaginary wavenumber axis.

The most dramatic alteration to the dispersion relation made by confinement is the creation of poles along the imaginary wavenumber axis. Near a pole at a finite

$\alpha = \alpha_p$, $\omega \to \infty$, and therefore the coefficient of $c$ in (1.2) tends to zero, giving

$$v'' - \alpha_p^2 v = 0. \tag{3.1}$$

While (1.3) only applies to regions of the flow where the basic flow $U$ has zero curvature, (3.1) applies to the whole of any flow independently of $U$ when $|c| \gg 1$. There are no nontrivial solutions to (3.1) satisfying $v \to 0$ at both $y \to \infty$ and $y \to -\infty$, and so there are no poles in the unconfined flow. However, there are nontrivial solutions to (3.1) satisfying the confined flow boundary conditions, $v(\pm h) = 0$, when

$$\alpha_p = \pm \frac{in\pi}{2h}, \quad \text{where } n = 1, 2, 3, \ldots. \tag{3.2}$$

Therefore, in the confined flow there are infinitely many poles along the imaginary wavenumber axis; they are $\pi/(2h)$ apart, and depend only on the separation of the plates, not on the flow between the plates. The corresponding expression for the poles for three-dimensional waves in a confined crossflow are given in (3.3) of Healey (2007), and in a cylindrical geometry for confined swirling jets they are found from zeros of the $J_1$ Bessel function (see (4.15) of Healey 2008).

In fact, the poles created by confinement correspond to acoustic modes in the compressible problem: the magnitude of the phase velocity $|c| \to \infty$ near a pole in the incompressible problem, and the waves are periodic in the cross-stream direction with an integer number of half-wavelengths fitting between the confining plates.

A pair of saddle points is associated with each pole. Even if the dispersion relation is almost non-dispersive in the unconfined flow, e.g. $\omega \sim a_1\alpha$, then a pole created by confinement at $\alpha = \alpha_p$ modifies the dispersion relation to $\omega \sim a_{-1}/(\alpha - \alpha_p) + a_1\alpha$, which has saddle points at $\alpha = \alpha_p \pm \sqrt{a_{-1}/a_1}$, which are close to the pole if $a_{-1}$ is small. These saddles created by confinement must be close to the poles when $h$ is large, since the poles lie on the imaginary wavenumber axis, and the dispersion relation is only affected by confinement close to the imaginary axis, i.e. for $\mathrm{Re}(\alpha) = O(h^{-1})$, so the confinement saddles are expected to lie no farther than $O(h^{-1})$ from the imaginary axis of the complex wavenumber plane. Asymptotic formulae for the saddle points and branch points surrounding each pole at large $h$ are presented in Healey (2007) for the rotating-disk boundary layer, but the heuristic arguments presented here describe the essence of the effect of confinement, which we now illustrate using a mixing-layer profile.

The Rayleigh equation (1.2) is solved numerically. The boundary conditions $v(\pm h) = 0$ are applied in the confined case. A solution $v_1$, with initial conditions $v_1(h) = 0$, $v_1'(h) = 1$, is integrated from $y = h$ to $y = 0$, and a solution $v_2$, with initial conditions $v_2(-h) = 0$, $v_2'(-h) = 1$, is integrated from $y = -h$ to $y = 0$. Roots of the dispersion relation are obtained by adjusting either $\alpha$ or $\omega$ until $v_1(0)/v_1'(0) = v_2(0)/v_2'(0)$ is satisfied within some small tolerance. The same procedure is followed in the unconfined case, but with initial conditions $v_1(h_0) = 1$, $v_1'(h_0) = -\alpha$ and $v_2(-h_0) = 1$, $v_2'(-h_0) = \alpha$, where $h_0 > 0$ is a large enough value for the basic velocity profile to be uniform at $y = \pm h_0$. These initial conditions force exponential decay of the solution with distance from the shear layer when $\mathrm{Re}(\alpha) > 0$.

Figure 3(*a*) shows the complex wavenumber plane for the unconfined mixing layer (2.10). There is a single saddle point, and at this value of $r$, the unconfined flow is convectively unstable since $\mathrm{Im}(\omega) < 0$ at the saddle point. Figure 3(*b*) shows the appearance of poles and saddles created by confinement. At this value of $h$, the

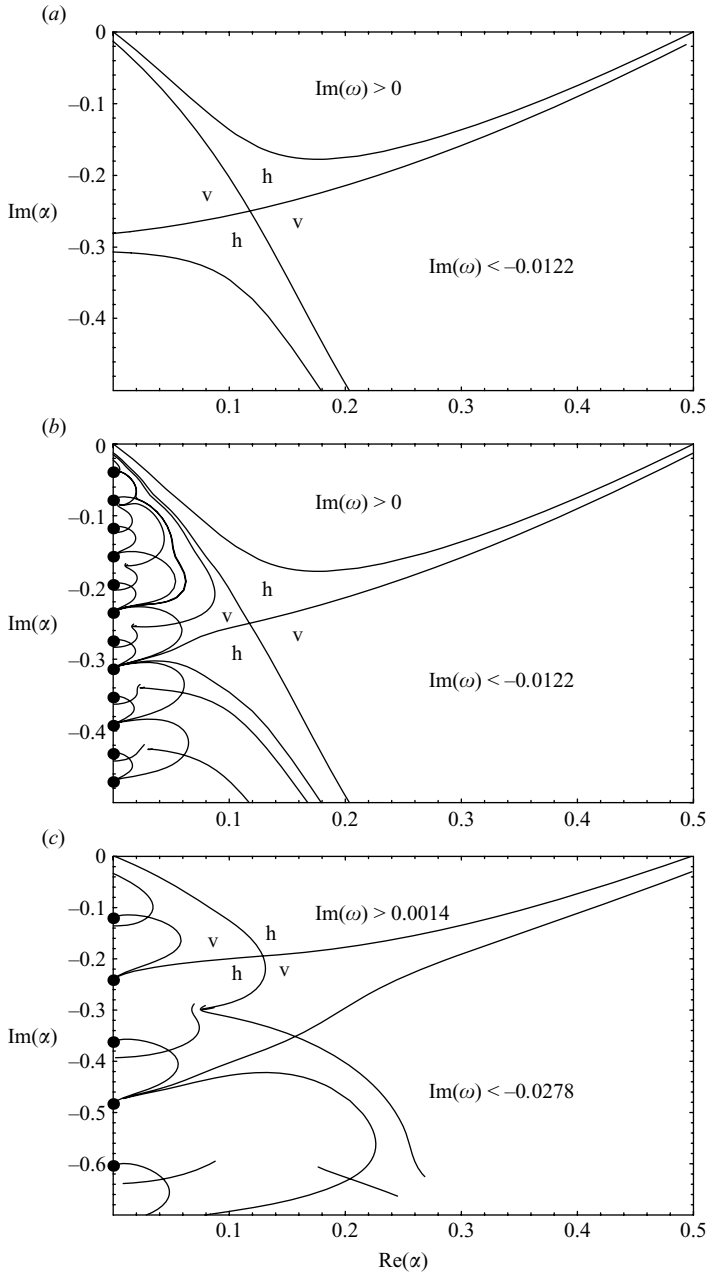


FIGURE 3. Contours of constant Im($\omega$) for the mixing layer (2.10) for $r = 1.25$. (*a*) Unconfined flow; (*b*) confined flow with $h = 40$; (*c*) confined flow with $h = 13$. In each case, the hills and valleys of the dominant saddle point (pinch point) are marked by h and v, respectively. Contours terminate when a critical point (at $y_c$ where $U(y_c) = c$) crosses the real $y$ axis. Disks on imaginary $\alpha$ axis are poles given by (3.2).

saddles are close enough to the imaginary $\alpha$ axis not to affect the saddle point of the unconfined flow, which remains the dominant saddle. However, as $h$ is reduced, the confinement saddle points move farther away from the imaginary $\alpha$ axis, and in figure 3(*c*) the flow is absolutely unstable with one of the confinement saddle

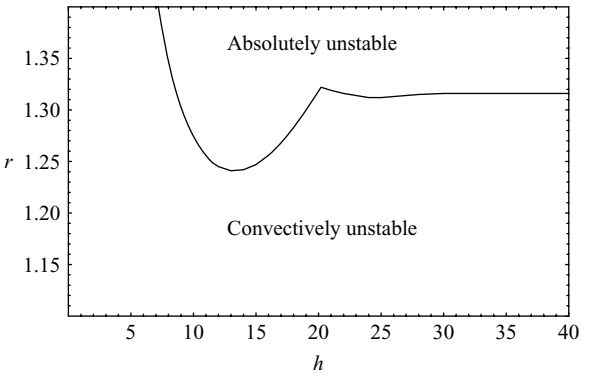


FIGURE 4. Neutral curve for absolute instability for the mixing layer (2.10) confined by plates at $y = \pm h$.

points becoming the dominant saddle point. Thus, confinement can create absolute instability.

Figure 4 shows the neutral curve for absolute instability for (2.10) with confinement. As $h \to \infty$, the neutral curve approaches the value $r = 1.316$, corresponding to that found by Huerre & Monkewitz (1985) for the onset of absolute instability in the unconfined flow. For $h < 20.2$, a confinement saddle point becomes the dominant saddle point, and for $8.7 < h < 19.8$ confinement makes the flow more absolutely unstable than the unconfined problem. It is only for $h < 8.7$ that the stabilizing effect of confinement seen on the temporal instability also stabilizes the absolute instability.

## 4. Absolute instability of asymmetrically confined mixing layers

In this section, we show that much stronger destabilization of the absolute instability is possible when the mixing layer is confined asymmetrically, i.e. when the mixing layer does not lie exactly halfway between the plates. We show first that this effect does not depend significantly on the shape of the velocity profile in the mixing layer when the plates are far apart by developing a long-wave theory for the arbitrary mixing layer (1.1).

When $h \to \infty$ the poles (3.2), with $n$ finite, approach the origin of the complex wavenumber plane, and so do the confinement saddle points associated with each pole. This means that in this limit the confinement saddle points can be described by a long-wave theory. It turns out that the leading-order dispersion relation of the long-wave theory captures the dominant saddle point (pinch point).

The linearized inviscid disturbance equations are obtained by substituting normal-mode forms for disturbances superimposed on the basic flow, $U(y)$,

$$\hat{u}(x, y, t) = U(y) + \delta u(y) \exp \mathrm{i}(\alpha x - \omega t), \tag{4.1a}$$

$$\hat{v}(x, y, t) = \delta v(y) \exp \mathrm{i}(\alpha x - \omega t), \tag{4.1b}$$

$$\hat{p}(x, y, t) = \delta p(y) \exp \mathrm{i}(\alpha x - \omega t), \tag{4.1c}$$

where $\hat{u}$, $\hat{v}$ and $\hat{p}$ are the velocity components in the $x$ and $y$ directions, and pressure, respectively, into the inviscid equations of motion, and linearizing in the small parameter $\delta$, which characterizes the amplitude of the wavy disturbances, to give

$$\mathrm{i}\alpha u + v' = 0, \tag{4.2a}$$

$$-\mathrm{i}\omega u + \mathrm{i}\alpha U u + U' v = -\mathrm{i}\alpha p, \tag{4.2b}$$

$$-\mathrm{i}\omega v + \mathrm{i}\alpha U v = -p'. \tag{4.2c}$$

The quantities $u$ and $p$ can be eliminated from (4.2) to give the Rayleigh equation, (1.2), but the long-wave theory follows more easily from (4.2).

Let $\epsilon \ll 1$ be a small parameter characterizing the smallness of the wavenumber. The separation of the plates (relative to the shear-layer thickness) is chosen to be of the order of the wavelength of disturbances so that confinement effects enter the problem at leading order. In the unconfined Kelvin–Helmholtz instability, $c = \omega/\alpha = O(1)$, and the same scaling applies in the confined problem. Therefore, the leading-order long-wave scalings are

$$\alpha = \alpha_0 \epsilon, \quad \omega = c_0 \alpha_0 \epsilon + \cdots \tag{4.3a, b}$$

and the boundary conditions are

$$v(h_1/\epsilon) = 0, \quad v(-h_2/\epsilon) = 0, \tag{4.4a, b}$$

where $h_1$ and $h_2$ are positive, and asymmetric confinement occurs when $h_1 \neq h_2$.

The disturbance equations (4.2) are solved using matched asymptotic expansions, in which the solution's slow exponential behaviour far from the shear layer, where the solution varies on the scale of the wavelength, is matched to a more rapid variation on the scale of the shear-layer thickness. The dispersion relation at leading order for (1.1) is found to be

$$[(c_0 - 1)^2 + r^2] \sinh \alpha_0 (h_1 + h_2) = 2r(c_0 - 1) \sinh \alpha_0 (h_2 - h_1) \tag{4.5}$$

(see Appendix B for details). It is important to note that, at this order, the dispersion relation is independent of $f(y)$; the dependence on the detail of the velocity profile is a higher-order effect. In fact, (4.5) is the dispersion relation that would be obtained by confining two uniform streams that are separated by a vortex sheet, i.e. $f(y) = 1$ for $y > 0$ and $f(y) = -1$ for $y < 0$.

The case of symmetric confinement, $h_1 = h_2$, is seen to be a degenerate case, reproducing the non-dispersive unconfined Kelvin–Helmholtz dispersion relation $c_0 = 1 \pm r\mathrm{i}$. However, any degree of asymmetry in the confinement, $h_1 \neq h_2$, makes the flow dispersive at leading order, and therefore gives the possibility of saddle points, and absolute instability, for mixing layers independently of their velocity profiles provided that the plate separation is sufficiently large.

Even though (4.5) was derived for small $\alpha$ and $c = O(1)$, (4.3), it correctly predicts the existence and location of poles in the complex wavenumber plane; poles, at which $|c_0| \to \infty$, occur at zeros of the coefficient of $c_0^2$ in (4.5), i.e. at

$$\alpha_p = \pm \frac{\mathrm{i}n\pi}{(h_1 + h_2)}, \quad \text{where } n = 1, 2, 3, \ldots, \tag{4.6}$$

in agreement with (3.2) where $h = h_1 = h_2$. As discussed in § 3, there are saddle points close to the poles, and figure 5 gives an example of the complex wavenumber plane for the asymmetrically confined mixing layer in the long-wave limit, showing saddle points created by confinement near the imaginary wavenumber axis. The dispersion relation (4.5) reduces to the non-dispersive unconfined Kelvin–Helmholtz dispersion relation when $\mathrm{Re}(\alpha_0)h_1 \gg 1$ and $\mathrm{Re}(\alpha_0)h_2 \gg 1$, because then $|\sinh \alpha_0(h_2 - h_1)| \ll \sinh \alpha_0(h_1 + h_2)$, and so contours of constant $\mathrm{Im}(\omega)$ become straight lines with gradient $-r$. These contours do not return to the real $\alpha$ axis for (4.5) because at this order there is no

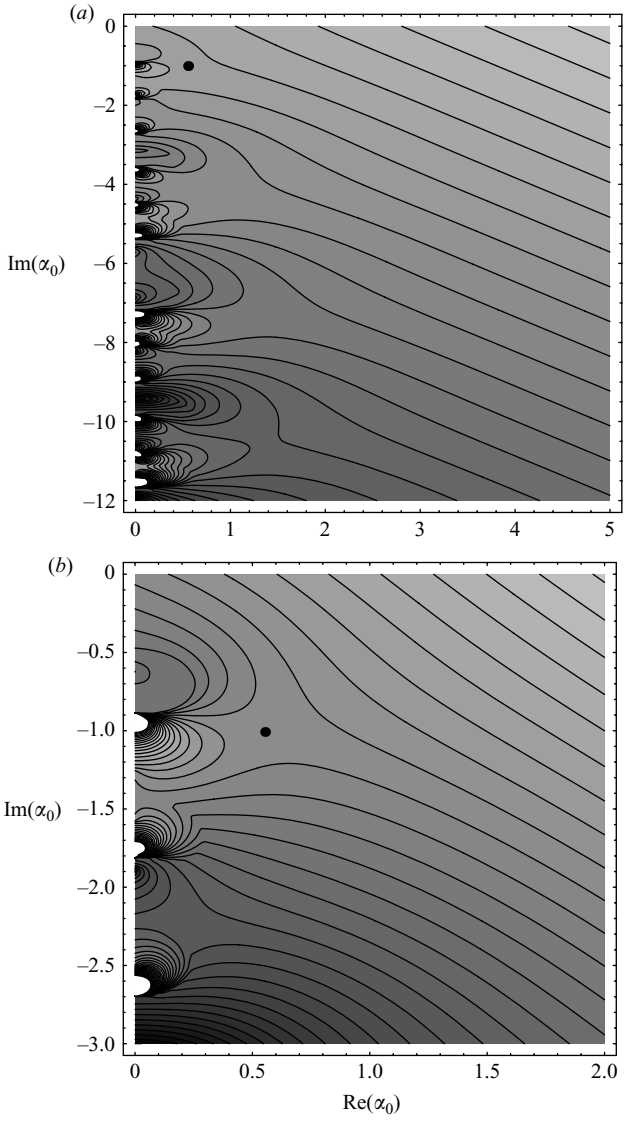


FIGURE 5. Contours of constant $\mathrm{Im}(\omega_0)$ in the complex $\alpha_0$ plane for the leading-order long-wave dispersion relation (4.5) for the asymmetric confinement $h_1 = 1$, $h_2 = 2.5$ and shear strength $r = 1$. The dominant saddle point (pinch point) is marked by the solid disk and lies at $\alpha_0 = 0.554 - 1.008\mathrm{i}$ and has $\omega_0 = 1.850 + 0.004\mathrm{i}$, corresponding to absolute instability. (*b*) is an enlargement of (*a*). Darker shades correspond to more negative $\mathrm{Im}(\omega_0)$, and lighter shades to more positive $\mathrm{Im}(\omega_0)$.

short-wave stabilization, which depends on the mixing layer having finite thickness; at leading order in the long-wave theory, the mixing layer has a negligible thickness compared to wavelength. Note also that the qualitative arrangement of contours in figure 5 depends only on $r$ and the ratio $h_2/h_1$; changing $h_1$ and $h_2$ at fixed $h_2/h_1$ only changes the scales on the axes of the complex wavenumber plane and the value of $\mathrm{Im}(\omega)$ on each contour.

Figure 5 shows that all shear layers with $r = 1$ are absolutely unstable for $h_2/h_1 = 2.5$ with finite positive $\mathrm{Im}(\omega)$, provided that the plates are far enough apart. Therefore,

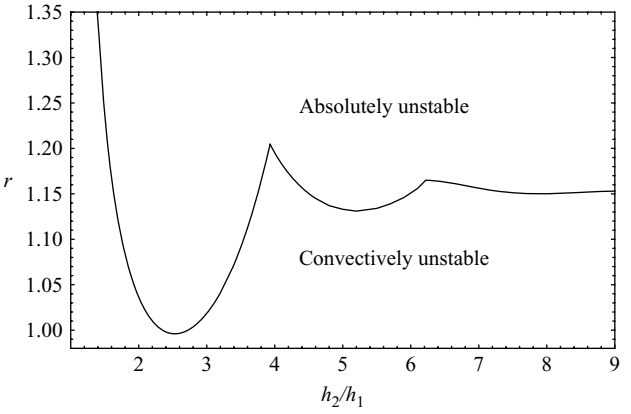


FIGURE 6. Neutral curve for absolute instability for the leading-order long-wave dispersion relation for asymmetric confinement (4.5). Discontinuities in gradient correspond to changes in dominance of saddle points.

co-flow shear layers with $r < 1$ can be absolutely unstable with suitable asymmetric confinement. Figure 6 shows the neutral curve for absolute instability in the long-wave limit. The minimum value of $r$ for absolute instability in this limit is $r = 0.996$, which occurs at $h_2/h_1 = 2.53$. There is co-flow absolute instability, i.e. $r < 1$, for $2.35 < h_2/h_1 < 2.72$, and the asymmetrically confined tanh profile, (2.10), is more absolutely unstable than the unconfined case for $h_2/h_1 > 1.42$, i.e. the neutral curve then lies in $r < 1.316$.

These long-wave results apply in the limit $h_1 \to \infty$ and $h_2 \to \infty$. Greater destabilization of the absolute instability occurs as $h_1$ and $h_2$ are reduced due to the same mechanism as described in § 3 where the confinement saddles move farther away from the imaginary wavenumber axis as the mixing layer becomes more strongly confined (see figure 3), leading to enhanced absolute instability at finite confinements (see figure 4). Figure 7 shows the extent of this additional destabilization effect at finite plate separations: at $h_1 = 15$, $h_2 = 2.53h_1$, the flow becomes absolutely unstable when $r = 0.934$. The long-wave dispersion relation (4.5) is shown to give good quantitative predictions for the dominant saddle point even when the plate separation is not especially large.

Figure 8 shows the complex wavenumber plane obtained from numerical solutions of the Rayleigh equation, (1.2), for the tanh profile, (2.10), for an asymmetric confinement. The dominant saddle point is the one nearest the real $\alpha$ axis, which is in agreement with the prediction made by the long-wave theory shown in figure 5. The qualitative arrangement of the saddle points nearest the real $\alpha$ axis in figure 8 is also very similar to those in figure 5. However, while the contours in figure 5 become parallel to $\mathrm{Im}(\alpha) = -r\,\mathrm{Re}(\alpha)$ as $\mathrm{Re}(\alpha)$ increases, in figure 8 they return to the real $\alpha$ axis because the finite thickness of the mixing layer (2.10) stabilizes sufficiently short waves.

In the long-wave limit the dispersion relation for asymmetric confinement of a mixing layer corresponds to that for varicose modes of the confined jet/wake flow considered by Juniper (2006). Figure 6 thus corresponds to Juniper's figure 11. Juniper provides an explanation for the multiple minima of the neutral curve in figure 6. A family of confinement saddle points can be associated with each plate. The distance of each family from the imaginary wavenumber axis, and the distance between them along the imaginary axis, scales inversely with the distance of each respective plate

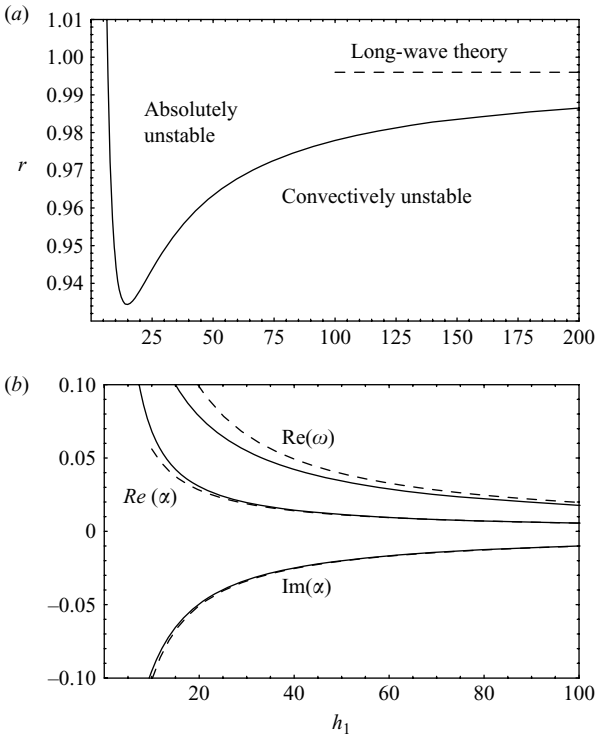


FIGURE 7. (*a*) Neutral curve for absolute instability for the asymmetrically confined tanh profile, (2.10), with $h_2 = 2.53h_1$ and $\epsilon = 1$ in (4.4). (*b*) Real and imaginary parts of the eigenvalues at the saddle point along the neutral curve shown in (*a*). In each diagram, solid lines correspond to numerical solutions of the Rayleigh equation, (1.2), and dashed lines to the leading-order long-wave theory, (4.5).

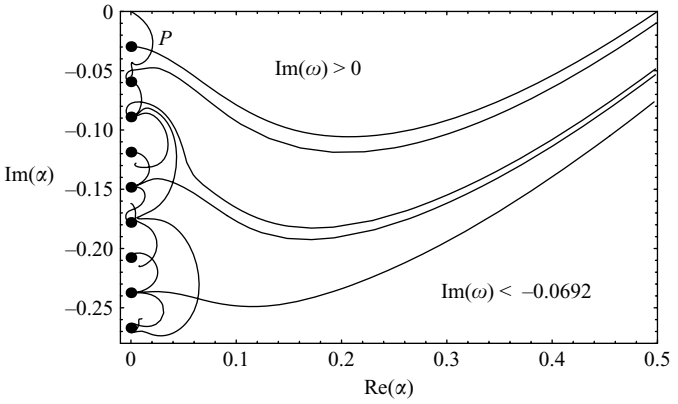


FIGURE 8. Complex wavenumber plane for the asymmetrically confined tanh profile, (2.10), at the point $h_1 = 30$, $h_2 = 2.53h_1$, $r = 0.9489$ on the neutral curve shown in figure 7(*a*). Solid disks are the poles predicted by (4.6) and the dominant saddle point (pinch point) is marked $P$.

from the mixing layer. It is found that when the plate separations are such that the saddle points of one family interact with saddle points of the other, then there is particular destabilization of the absolute instability giving local minima of the neutral curve in figure 6. Physically, this interaction corresponds to when the cross-stream

wavelengths in the streams on either side of the mixing layer match, leading to a kind of constructive interference.

## 5. Dependence of absolute instability on the velocity profile with symmetric confinement

We now return to the case of symmetric confinement studied in § 3 where it was shown that a range of finite plate separations could destabilize the absolute instability of the tanh mixing-layer profile (2.10) when the plates are equidistant from the mixing layer. The discussion in § 4 shows that certain asymmetric confinements cause significantly greater destabilization of the absolute instability, such that even co-flow mixing layers become absolutely unstable. Furthermore, it was shown that this effect persists even when the plate separation is arbitrarily large.

It was also noted in § 4 that symmetric confinement is a degenerate case in the long-wave limit, with dispersion only appearing as a higher-order correction in the theory. The results for symmetric confinement are therefore expected to be sensitive to the particular shape of the velocity profile. In the present section, we show that this is indeed the case, and identify a class of modifications to the basic velocity profile that substantially enhances absolute instability in the presence of symmetric confinement, to the extent that co-flow absolute instability is possible in this case too, for carefully chosen profiles and plate separations.

The nature of the modifications to the basic velocity profile that can enhance the absolute instability can be found by considering the second-order long-wave dispersion relation for the symmetrically confined mixing layer because this provides an analytical expression for confinement saddle points that explicitly includes the basic velocity profile. Although this theory applies in the limit $h \to \infty$, and figure 4 shows that confinement saddle points are only dominant at finite values of $h$ ($h < 20.2$ for the tanh profile 2.10), we find that the theory does give practical insights into how modifications to the basic velocity profile affect absolute instability when the mixing layer is symmetrically confined.

### 5.1. *Long-wave theory for weakly confined mixing layers*

The leading-order expansions (4.3) are extended to

$$\alpha = \alpha_0 \epsilon, \quad \omega = \alpha_0 \epsilon (c_0 + c_1 \epsilon + \cdots) \tag{5.1a, b}$$

and the boundary conditions are

$$v(\pm h_0/\epsilon) = 0. \tag{5.2}$$

Setting $h_1 = h_2 = h_0$ in (4.5), we find that the unstable solution of the leading-order dispersion relation is $c_0 = 1 + r\mathrm{i}$, i.e. the non-dispersive unconfined Kelvin–Helmholtz instability. The dispersion relation at next order is found to be

$$c_1 = \frac{\mathrm{i}}{4} r \alpha_0 I_1 \tanh(\alpha_0 h_0) + \mathrm{i} r \alpha_0 I_2 \coth(\alpha_0 h_0), \tag{5.3}$$

where the dependence on the basic flow, (1.1), enters through the integrals

$$I_1 = \int_{-\infty}^{\infty} [f(t) - \mathrm{i}]^2 \, \mathrm{d}t, \quad I_2 = \int_{-\infty}^{\infty} \frac{1}{[f(t) - \mathrm{i}]^2} \, \mathrm{d}t \tag{5.4a, b}$$

(see Appendix C for details). This second-order theory correctly predicts the existence of poles at $\alpha_0 = \pm \mathrm{i} n \pi / (2 h_0)$ for $n = 1, 2, 3, \ldots$ in agreement with (3.2).

The condition for a saddle point, $\mathrm{d}\omega/\mathrm{d}\alpha = 0$, can now be written using (5.1) as

$$0 = \frac{\mathrm{d}}{\mathrm{d}\alpha_0}[\alpha_0(c_0 + \epsilon c_1 + \cdots)]$$

$$\Rightarrow \quad 0 = 1 + r\mathrm{i} + \mathrm{i}\epsilon r\alpha_0 \left[\frac{I_1}{2}\tanh(\alpha_0 h_0) + 2I_2\coth(\alpha_0 h_0) + \frac{\alpha_0 h_0 I_1}{4}\mathrm{sech}^2(\alpha_0 h_0) - \alpha_0 h_0 I_2 \mathrm{cosech}^2(\alpha_0 h_0)\right]. \tag{5.5}$$

Equation (5.5) has roots when a term in the square brackets is $O(\epsilon^{-1})$. This occurs when either $\sinh(\alpha_0 h_0)$ or $\cosh(\alpha_0 h_0)$ is small, i.e. near poles. In particular, at a saddle point, $\alpha_0 = \pm\, \mathrm{i}n\pi/(2h_0) + O(\epsilon^{-1/2})$. There are two cases depending on whether $n$ is odd or even

$$\alpha = \epsilon\alpha_0 \sim \frac{(2m+1)\pi\mathrm{i}\epsilon}{2h_0}\left\{1 \pm \left[\frac{\mathrm{i}r I_1\epsilon}{4h_0(1+\mathrm{i}r)}\right]^{1/2}\right\} \tag{5.6a}$$

$$\Rightarrow \quad \omega \sim \frac{(2m+1)\pi\mathrm{i}\epsilon}{2h_0}(1+\mathrm{i}r)\left\{1 \pm \left[\frac{\mathrm{i}r I_1\epsilon}{h_0(1+\mathrm{i}r)}\right]^{1/2}\right\}, \tag{5.6b}$$

i.e. $n = 2m + 1$, and

$$\alpha = \epsilon\alpha_0 \sim \frac{m\pi\mathrm{i}\epsilon}{h_0}\left\{1 \pm \left[\frac{\mathrm{i}r I_2\epsilon}{h_0(1+\mathrm{i}r)}\right]^{1/2}\right\} \tag{5.7a}$$

$$\Rightarrow \quad \omega \sim \frac{m\pi\mathrm{i}\epsilon}{h_0}(1+\mathrm{i}r)\left\{1 \pm \left[\frac{4\mathrm{i}r I_2\epsilon}{h_0(1+\mathrm{i}r)}\right]^{1/2}\right\}, \tag{5.7b}$$

i.e. $n = 2m$, where in each case $m$ is a negative integer for the confinement saddle points lying near the negative imaginary $\alpha$ axis, which figure 3 shows can form pinch points when $h$ is not too large. In fact, figure 3($c$) shows that it is the $n = -2$, i.e. $m = -1$ of (5.7), saddle point that becomes the pinch point for finite $h$, because the pinch point in the figure is associated with the second pole down from the origin of the complex wavenumber plane.

The results for the saddle points in the large $h$, long-wave, limit (5.6) and (5.7), confirm that at large enough $h$ symmetric confinement does not produce absolute instability because in both (5.6$b$) and (5.7$b$), $\mathrm{Im}(\omega) \to n\pi/(2h)$, as $\epsilon \to 0$, which is negative for $n < 0$. However, at finite $h$, figure 4 shows that the confinement saddle points can produce absolute instability, and the $O(\epsilon^{1/2})$ corrections shown in (5.6) and (5.7) indicate the destabilizing effects as $h$ is reduced, i.e. as $\epsilon$ increases.

The influence of the basic flow, $f(y)$, on the absolute instability enters through the integrals $I_1$ and $I_2$, and the growth rate of the saddle points depends on both the modulus and argument of these complex quantities. The real and imaginary parts of these integrals are

$$I_1 = \int_{-\infty}^{\infty} f(t)^2 - 1\,\mathrm{d}t - \mathrm{i}\int_{-\infty}^{\infty} 2f(t)\,\mathrm{d}t, \tag{5.8a}$$

$$I_2 = \int_{-\infty}^{\infty} \frac{f(t)^2 - 1}{[f(t)^2+1]^2}\,\mathrm{d}t + \mathrm{i}\int_{-\infty}^{\infty} \frac{2f(t)}{[f(t)^2+1]^2}\,\mathrm{d}t. \tag{5.8b}$$

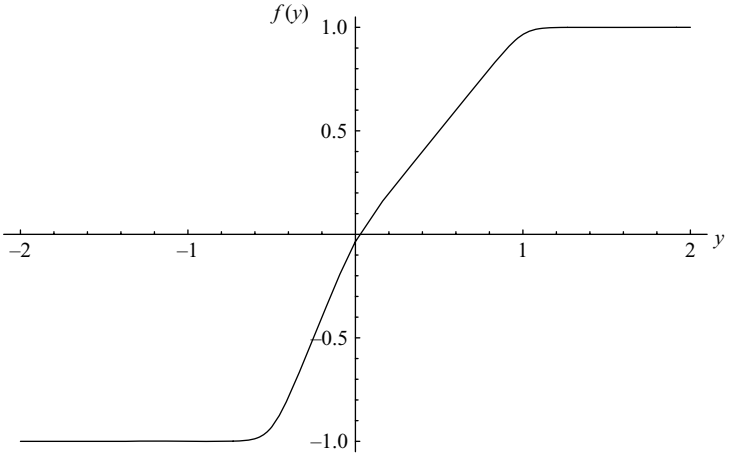


FIGURE 9. Asymmetric shear layer (5.9) with $\phi = 2$ and $\delta = 0.1$.

Therefore, both integrals are real when $f$ is an odd function, such as (2.10), but become complex when $f$ is not an odd function. Therefore, breaking the symmetry $f(-y) = -f(y)$ directly modifies the growth rate of the confinement saddle points, and offers the possibility of further enhancing the absolute instability.

### 5.2. *Absolute instability of asymmetric mixing-layer profiles*

The following velocity profile has parameters that control the strength of the profile asymmetry, and therefore the size and sign of the imaginary parts of the integrals $I_1$ and $I_2$, which in turn modify the growth rate of the confinement saddle points,

$$f(y) = \frac{\delta}{2}\left(\phi \log\left\{\frac{\cosh[(1+\phi y)/(\phi\delta)]}{\cosh(y/\delta)}\right\} + \log\left\{\frac{\cosh(y/\delta)}{\cosh[(y-1)/\delta]}\right\}\right). \tag{5.9}$$

In the limit $\delta \to 0$ (5.9) approaches the piecewise-linear profile

$$f(y) = \begin{cases} 1 \text{ for } & 1 \leqslant y \\ y \text{ for } & 0 \leqslant y < 1 \\ \phi y \text{ for } & -1/\phi \leqslant y < 0 \\ -1 \text{ for } & y < -1/\phi \end{cases}. \tag{5.10}$$

Thus, the parameter $\phi$ controls the asymmetry of the mixing layer: $\phi = 1$ causes $f(-y) = -f(y)$; $\phi > 1$ causes the shear to be greater towards the slower stream; $\phi < 1$ causes the shear to be greater towards the faster stream. The parameter $\delta$ characterizes the distance over which each of the four layers in (5.10) merges into its adjacent layers. In the limit $\delta \to \infty$ and $\phi = 1$, (5.9) approaches $f(y) = \tanh(y/\delta)$. Figure 9 illustrates (5.9) for a particular pair of values of $\phi$ and $\delta$.

By making suitable choices for $\phi$ and $\delta$, and also the symmetric confinement parameter $h$, it is possible to destabilize the absolute instability sufficiently to obtain co-flow absolute instability, i.e. for $r < 1$. Figure 10 shows an example of the complex wavenumber plane for co-flow absolute instability obtained from numerical solutions of the Rayleigh equation. Note that, as for the symmetrically confined tanh profile (2.10) (see figure 3), the pinch point in figure 10 also corresponds to the second pole down from the origin, i.e. $m = 1$ in (5.7). In this example, the mixing layer is relatively strongly confined, and the boundary layers on the confining plates might be expected

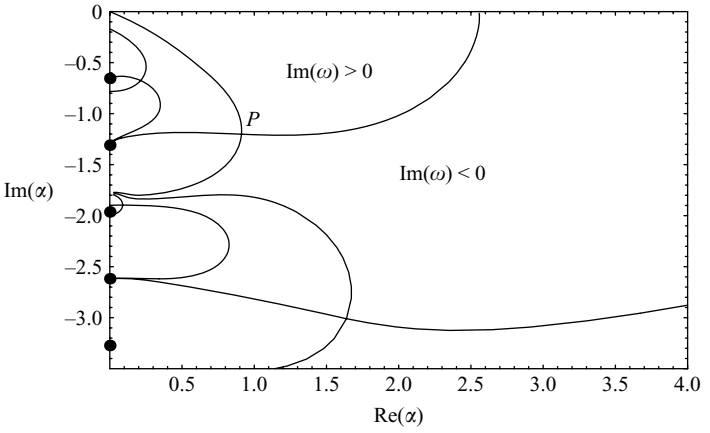


FIGURE 10. Contours of constant $\mathrm{Im}(\omega)$ for the asymmetric shear layer (5.9) with $\phi = 1.6$, $\delta = 0.02$, $h = 2.4$ and $r = 0.99003$. The solid disks represent the poles (3.2). At the pinch point, marked by a $P$, $\alpha = 0.912 - 1.201\mathrm{i}$ and $\omega = 0.759$. This flow is absolutely unstable for $r > 0.99003$.

to affect the absolute instability, even though instabilities associated with boundary layers are generally weaker than those associated with mixing layers.

In fact, asymmetry in the mixing-layer profile is a common feature in experiments, and would be produced, for example, by the wake behind a splitter plate. This asymmetry can be further strengthened if the boundary-layer thickness on one side of the splitter plate is different from the boundary-layer thickness on the other side. This will generally be the case because the flow velocity is different on either side of the splitter plate. However, such an asymmetry will decay with distance downstream from the splitter plate.

We note that Koch (1985) also considered asymmetric wake profiles, but he found stabilization rather than destabilization. The results in this section for mixing layers, guided by the long-wave theory, indicate that although destabilization by profile asymmetry can be large enough to produce a co-flow absolute instability, it only does so for carefully chosen profiles and confinements.

## 6. Absolute instability of semiconfined mixing layers

The absolute instability of the mixing layer is also affected by adding just a single plate. We call this case 'semiconfinement'; the flow is still taken to be of infinite extent on one side of the mixing layer, but of finite extent on the other side. For example, if a plate is added at $y = h > 0$, then the boundary conditions become

$$v(h) = 0, \qquad \lim_{y \to -\infty} (v' - \alpha v) = 0. \tag{6.1a, b}$$

It is helpful to consider the long-wave dispersion relation for this case,

$$[(c_0 - 1)^2 + r^2] \exp(\alpha_0 h_0) = 2r(c_0 - 1) \exp(-\alpha_0 h_0), \tag{6.2}$$

where the long-wave scalings (4.3) apply, and the plate is placed at $y = h_0/\epsilon$ (see Appendix D for details). The non-dispersive unconfined Kelvin–Helmholtz result, $c_0 = 1 \pm r\mathrm{i}$, is recovered when $\mathrm{Re}(\alpha_0)h_0 \gg 1$, but the exponential terms in (6.2) are oscillatory near the imaginary $\alpha_0$ axis, and this leads to the appearance of an infinite number of saddle points near this imaginary axis (see figure 11 for an example showing

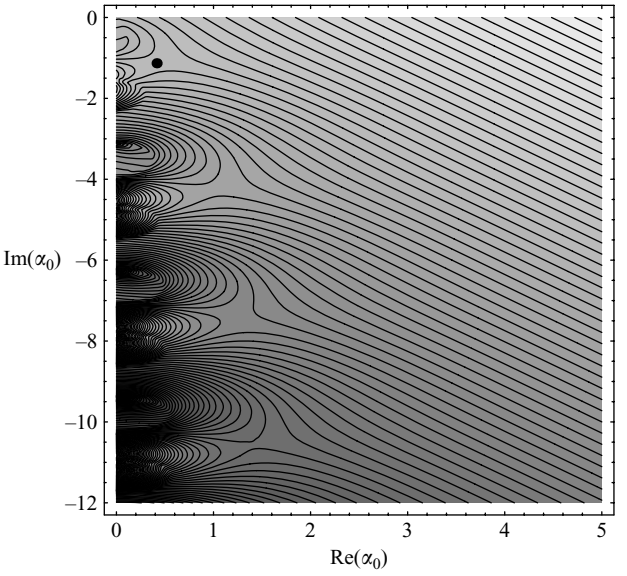


FIGURE 11. Contours of constant $\mathrm{Im}(\omega_0)$ in the complex $\alpha_0$ plane for the leading-order long-wave dispersion relation (6.2) for the semiconfinement $h_0 = 1$ and shear strength $r = 1.153$. The dominant saddle point (pinch point), marked by a solid black disk, lies at $\alpha_0 = 0.414 - 1.132\mathrm{i}$ and has $\omega_0 = \alpha_0 c_0 = 2.009$. There is absolute instability for $r > 1.153$. Darker shades correspond to more negative $\mathrm{Im}(\omega_0)$, and lighter shades to more positive $\mathrm{Im}(\omega_0)$.

the start of the sequence of saddle points that lie to the right of the negative imaginary $\alpha_0$ axis). Note that the qualitative arrangement of the contours is independent of $h_0$ in this leading-order dispersion relation; changing $h_0$ only rescales the axes of the diagram and the values on contours.

Although semiconfinement does not replace the imaginary axis branch cut with poles (the coefficient of $c_0^2$ in 6.2 is always non-zero, so there are no solutions with $|c_0| \to \infty$), it generates an infinite number of saddle points near the imaginary wavenumber axis. They correspond to columnar modes in the uniform flow between the mixing layer and the confining plate whose cross-stream wavelengths are compatible with the distance between the mixing layer and plate. These modes are not present in boundary-layer flows, even though these flows might be regarded as semiconfined shear layers, because they depend on there being a region of uniform flow between the shear layer and plate that is significantly larger than the shear-layer thickness.

The key observation to be made from figure 11 is that semiconfinement creates a saddle point with $\mathrm{Im}(\omega_0) > 0$ at lower values of $r$ than required for absolute instability in the unconfined case. Therefore, semiconfinement by a plate in the faster stream enhances absolute instability provided the plate is far from the mixing layer, and in this limit the effect is independent of the detail of the velocity profile. In fact, the threshold for absolute instability in the semiconfined problem, $r = 1.153$, gives the horizontal asymptote of the neutral curve for asymmetric confinement as $h_2/h_1 \to \infty$ that can be seen developing in figure 6. Figure 12 shows that this destabilization becomes stronger as the plate approaches the mixing layer, leading to absolute instability at $r = 1.005$, $h = 11$, for the tanh profile (2.10).

However, semiconfinement by placing a plate in the slower stream is found to stabilize the absolute instability. One can either modify the boundary conditions (6.1)

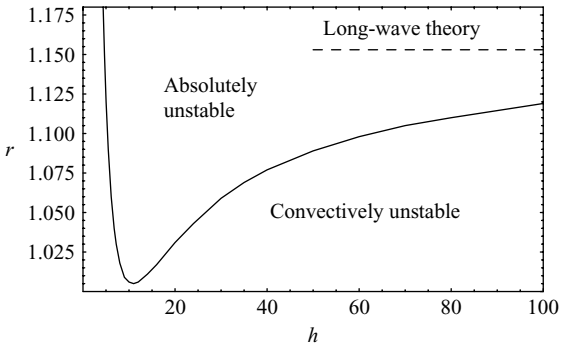


FIGURE 12. Solid line is the neutral curve for absolute instability for the semiconfined tanh profile, (2.10), obtained from numerical solutions of the Rayleigh equation (1.2) with boundary conditions (6.1). Dashed line is the large $h$, long-wave, asymptote to this neutral curve obtained from (6.2), i.e. $r = 1.153$.

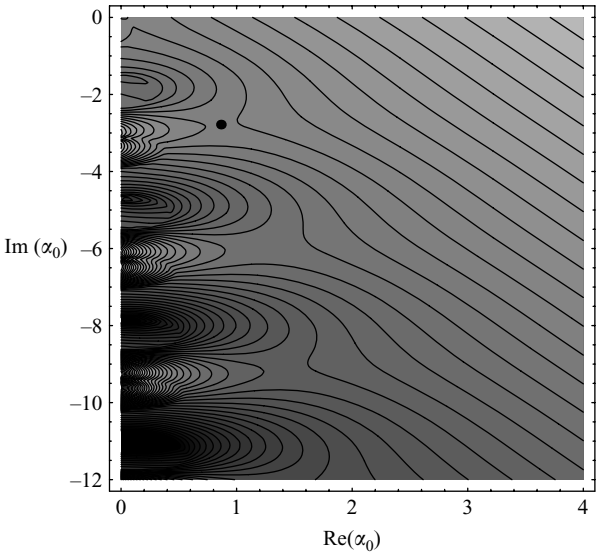


FIGURE 13. Contours of constant $\mathrm{Im}(\omega)$ in the complex $\alpha_0$ plane for the leading-order long-wave dispersion relation (6.2) for the semiconfinement $h_0 = 1$ and shear strength $r = -2.018$, i.e. with the plate placed in the slower stream. The dominant saddle point, marked by the solid black disk, lies at $\alpha_0 = 0.864 - 2.782\mathrm{i}$ and has $\omega_0 = \alpha_0 c_0 = 6.864$. This saddle has $\mathrm{Im}(\omega_0) > 0$ for $r < -2.018$. Darker shades correspond to more negative $\mathrm{Im}(\omega_0)$, and lighter shades to more positive $\mathrm{Im}(\omega_0)$. There is no saddle near $\alpha = 0.06 - 0.2\mathrm{i}$, the contours in this region have jumped from one solution for $c_0$ from (6.2) to the other.

to $v(-h) = 0$, $\lim_{y\to\infty}(v' + \alpha v) = 0$, or, more simply, retain (6.1) and consider $r < 0$, which swaps over the faster and slower streams (see (1.1)). Figure 13 shows saddle points near the negative imaginary $\alpha_0$ axis created by semiconfinement due to a plate in the slower stream. The principal difference between this case and that shown in figure 11 is that here a stronger shear strength, $|r|$, is needed to destabilize these saddle points, i.e. $\mathrm{Im}(\omega) > 0$ only for $-r > 2.018$.

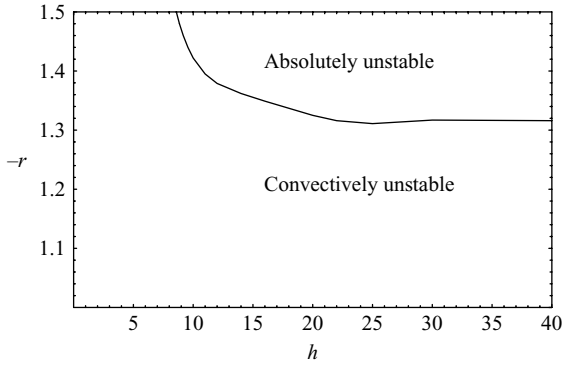


FIGURE 14. Solid line is the neutral curve for absolute instability for the semiconfined tanh profile, (2.10), obtained from numerical solutions of the Rayleigh equation (1.2) with boundary conditions (6.1). $r < 0$ corresponds to placing the plate in the slower stream.

Semiconfinement by a plate in the slower stream corresponds to the limit $h_2/h_1 \to 0$ with $r > 0$ in the asymmetrically confined case. Therefore, there is a second neutral curve for $h_2/h_1 < 1$ in figure 6 that asymptotes towards $r = 2.018$ as $h_2/h_1 \to 0$. This critical value of $r$ is larger than the shear strength that produces absolute instability in the unconfined case ($r = 1.316$). Therefore, in the case of semiconfinement with the plate placed in the slower stream, the saddle point of the unconfined problem remains the pinch point. Figure 14 shows the neutral curve for finite semiconfinement for the tanh profile with a plate in the slower stream. As $h \to \infty$, the neutral curve is seen to asymptote towards the result for unconfined flow, as in figure 4. As $h$ is reduced, there is increasing stabilization of the absolute instability by semiconfinement.

These results agree with those of Yu & Monkewitz (1990) because in the long-wave limit, the dispersion relation for semiconfinement of a mixing layer with the plate in the faster stream corresponds to an unconfined jet, and when the plate is in the slower stream it corresponds to an unconfined wake. Yu & Monkewitz found that jets are more absolutely unstable than wakes.

## 7. Conclusions

### 7.1. *General comments*

Confinement of a mixing layer has a relatively straightforward effect on its temporal stability. It exerts a stabilizing influence. This influence diminishes as the confining plates are moved farther from the mixing layer. This behaviour has been known since the work of Rayleigh (1894). The effects of semiconfinement (by a single plate), symmetric confinement (by plates equidistant from the mixing layer) and asymmetric confinement (by plates at unequal distance from the mixing layer) were studied in § 2. Semiconfinement has the weakest stabilizing effect, symmetric confinement is more stabilizing and asymmetric confinement is the most stabilizing. However, the neutral curves for all these types of confinements asymptote towards the unconfined case exponentially fast as the plates are moved away. These results underpin the pervasive intuition that the presence of confinement can be ignored in many circumstances.

It is surprising, then, to discover that confinement can have a strong destabilizing effect on a mixing layer's absolute instability characteristics even when the plates are arbitrarily far from the mixing layer.

The strongest destabilizing effect of confinement was found for asymmetric confinement when $h_2 = 2.53h_1$, where $h_2$ is the distance of the plate in the slower stream from the mixing layer, and $h_1$ is the distance of the plate in the faster stream from the mixing layer (see § 4). In fact, for $2.35 < h_2/h_1 < 2.72$ there is co-flow absolute instability when the plates are far enough apart regardless of the form of the mixing-layer velocity profile (see figure 6). The absolute instability can be further enhanced by bringing the plates closer to the mixing layer. For example, placing plates at $h_1 = 15$, $h_2 = 2.53h_1$ for the mixing layer (2.10) gives absolute instability when $r > 0.934$ ($r < 1$ gives co-flow, $r > 1$ gives counter flow).

Long-wave theories have been used to determine the circumstances when the absolute instabilities are influenced by the details of the velocity profile and when they are not. The long-wave theories also determine when the neutral curve for absolute instability of a confined flow asymptotes towards the neutral curve for absolute instability of the corresponding unconfined flow as the plates are moved away from the mixing layer, and when they do not. For example, for the unconfined mixing layer (2.10), the neutral curve for absolute instability is $r = 1.316$, but the neutral curve for the asymmetrically confined case asymptotes towards a value of $r < 1.316$ when $h_2/h_1 > 1.42$. The case of symmetric confinement, $h_2 = h_1$, therefore lies in the range where the neutral curve for absolute instability asymptotes towards the neutral curve for the unconfined flow, as illustrated in figure 4.

In fact, the long-wave theories reveal that symmetric confinement is a special case. At leading order, the symmetrically confined flow has the same dispersion relation as the unconfined flow, and is non-dispersive. Dispersion is an essential ingredient of absolute instability, and there are no saddle points in the long-wave limit for unconfined mixing layers (the long-wave dispersion relation is $c = \mathrm{d}\omega/\mathrm{d}\alpha = 1 \pm r\mathrm{i} \neq 0$). The dispersion behind the absolute instabilities for asymmetric confinement is due to the asymmetry of the confinement and is independent of the velocity profile. However, dispersion only arises as a higher-order effect in the symmetrically confined case, and at this order the dispersion relation depends on the mixing-layer velocity profile. Therefore, absolute instability in symmetrically confined and unconfined mixing layers depends sensitively on the basic velocity profile. A second-order long-wave theory developed in § 5 for symmetric confinement indicates that breaking the $f(-y) = -f(y)$ symmetry can destabilize the absolute instability, and indeed we were able to find a carefully chosen velocity profile that admits co-flow absolute instability for a certain finite range of confinement.

Like asymmetric confinement, the case of semiconfinement also generates dispersion at leading order in the long-wave limit. In § 6 we show that semiconfinement by a plate in the faster stream enhances the absolute instability and produces absolute instability for $r > 1.153$ regardless of the mixing-layer profile when the plate is far enough away from the mixing layer. For the case of the tanh profile, (2.10), semiconfinement produces absolute instability for $r > 1.005$ when $h = 11$. Co-flow absolute instability could be possible for a semiconfined mixing layer for a suitably chosen profile and confinement.

On the other hand, semiconfinement by a plate placed in the slower stream has a stabilizing effect on the absolute instability, and this could provide a means for substantially suppressing absolute instability in mixing layers.

Semiconfinement represents limiting cases of asymmetric confinement. Semiconfinement by a plate placed in the faster stream corresponds to asymmetric confinement as $h_2/h_1 \to \infty$ and by a plate placed in the slower stream it corresponds to asymmetric confinement as $h_2/h_1 \to 0$.

### 7.2. *A mechanism for destabilization and stabilization by semiconfinement*

Given that asymmetric confinement is the most stabilizing case for temporal instability, it is curious that it should turn out to be the most destabilizing case for absolute instability. Michael McIntyre (personal communication) has suggested a mechanism that might underlie this behaviour. Consider Rayleigh's piecewise-linear mixing-layer profile

$$f(y) = \begin{cases} 1 & \text{for } y > 1 \\ y & \text{for } -1 < y < 1 \\ -1 & \text{for } y < -1 \end{cases} \tag{7.1}$$

substituted into (1.1). A derivation of the dispersion relation for the unconfined problem can be found in Drazin & Reid (1981). In our variables, it is

$$c = 1 \pm \frac{r}{2\alpha}[(1-2\alpha)^2 - \exp(-4\alpha)]^{1/2}, \tag{7.2}$$

which in the long-wave limit (small $\alpha$) reduces to $c \sim 1 \pm r\mathrm{i}$. In the short-wave limit (large $\alpha$) the joins in the segments at $y = \pm 1$ act as waveguides and there are two neutral branches to the dispersion relation, with a faster wave travelling at almost the speed of the faster stream, and a slower wave travelling at almost the speed of the slower stream,

$$c \sim 1 + r - \frac{r}{2\alpha}, \quad c \sim 1 - r + \frac{r}{2\alpha}. \tag{7.3a, b}$$

The waves are non-dispersive in this limit too; they only see the jump in basic vorticity at a join, which has no natural length scale. However, there is dispersion if a confining plate is close enough to a join. Therefore, consider disturbances to (7.1) satisfying boundary conditions $v(1+h_1\epsilon) = v(-1-h_2\epsilon) = 0$ with $\alpha = \alpha_0/\epsilon$ and $\epsilon \ll 1$. We find

$$c \sim 1 + r - \frac{\epsilon r}{2\alpha_0}[1 - \exp(-2\alpha_0 h_1)], \quad c \sim 1 - r + \frac{\epsilon r}{2\alpha_0}[1 - \exp(-2\alpha_0 h_2)], \tag{7.4a, b}$$

and the group velocities of these waves are

$$\frac{\mathrm{d}\omega}{\mathrm{d}\alpha} \sim 1 + r - \epsilon r h_1 \exp(-2\alpha_0 h_1), \quad \frac{\mathrm{d}\omega}{\mathrm{d}\alpha} \sim 1 - r + \epsilon r h_2 \exp(-2\alpha_0 h_2). \tag{7.5a, b}$$

Therefore, the plate near the join at $y = 1$ slows down the mode associated with this waveguide, (7.5*a*), and the plate near the join at $y = -1$ speeds up the mode associated with this waveguide, (7.5*b*). The Kelvin–Helmholtz instability arises at the coalescence of these two neutral waveguide modes as their wavelengths increase, i.e. when the square bracket in (7.2) vanishes, leading to a complex conjugate pair of branches to the dispersion relation, and hence temporal instability. Absolute instability is associated with points of zero-group velocity, so it may be that placing a plate near the mixing layer in the faster stream, which slows down the faster mode, while placing the plate in the slower stream far from the mixing layer or removing it completely, so as not to speed up the slower mode, has the net effect of tending to reduce the group velocity, and thus promote absolute instability.

This mechanism is consistent with our observations that (i) asymmetric confinement is destabilizing for a certain range of $h_1 < h_2$, (ii) semiconfinement is destabilizing when the plate in the slower stream is removed and (iii) it is stabilizing when the plate in the faster stream is removed. However, it does not explain all of our observations; for example, the neutral curve for asymmetric confinement does not tend towards the semiconfinement case monotonically as $h_2/h_1 \to \infty$, and as noted above, the strongest

destabilization was found for $h_2 = 2.53h_1$. Also, $h_2/h_1$ must exceed a threshold before destabilization occurs; for the tanh profile (2.10) this threshold is $h_2 > 1.42h_1$.

These limitations are presumably related to the fact that this mechanism for slowing the faster waveguide mode operates in the short-wave limit, while the absolute instability is found to be destabilized by saddle points created by confinement near the imaginary wavenumber axis, and when the branches form a complex conjugate pair it is no longer possible to identify explicitly a faster and slower waveguide mode.

### 7.3. *Relationship between mixing-layer results and jet/wake results*

In the long-wave limit, the semiconfined mixing layer considered here corresponds to varicose modes of the three-layered piecewise-linear model of the unconfined jet/wake flow investigated by Yu & Monkewitz (1990). The confined mixing layer in the long-wave limit corresponds to the varicose modes of the confined jet/wake flow investigated by Juniper (2006). Consequently, Juniper's figure 11 corresponds to our figure 6. The non-monotonic behaviour of this neutral curve is explained by Juniper in terms of interactions between families of saddle points associated with each of the confining plates. The elimination of absolute instability at $h = 1$ in Juniper's figure 11 corresponds to the absence of absolute instability in the non-dispersive leading-order long-wave limit of the symmetrically confined mixing layer. However, this flow is absolutely unstable when one considers a realistic smooth velocity profile, as in Huerre & Monkewitz (1985). Therefore, if smooth profiles are used for the jet/wake velocity profiles instead of the piecewise linear profiles, then another saddle point will appear and produce absolute instability when Juniper's $h$ (a ratio of fluid layer thicknesses) is close to unity. Similar modifications would be present in Juniper's figure 15, which shows neutral curves for absolute instability over a range of density ratios, and which also has absolute instability disappearing at $h = 1$.

The additional destabilization seen in our study at finite plate separations for smooth profiles relative to the long-wave results at asymptotically large plate separations for discontinuous profiles, e.g. in our figures 7 and 12, would also act to extend the absolutely unstable parameter regions in Juniper's figures 11 and 15.

### 7.4. *Potential effects of viscosity*

We conclude with some remarks concerning how the present inviscid results might be affected by viscosity. The overall picture should not be modified much by small viscosity, and in many mixing-layer flows the Reynolds number is relatively large. The application of non-slip boundary conditions at the confining plates will generate boundary layers adjacent to the plates. However, boundary-layer instabilities are typically weaker than mixing-layer instabilities, so provided the boundary-layer thicknesses are small compared to the distances from the plates and the mixing layer, their presence should only make a small change to the stability characteristics. The possibility that the boundary layers could nonetheless significantly affect the propagation of disturbances is not so easily ruled out. After all, as we have illustrated in this paper, confinement can have a negligible effect on temporal stability while strongly affecting absolute instability, and so in principle, other small modifications, like small viscosity, might do likewise. A viscous calculation would seem to be necessary to settle the matter. However, the strong role of confinement was anticipated because the pinch point in the unconfined problem lies relatively close to the imaginary wavenumber axis, and this part of the wavenumber plane is strongly affected by confinement. There appears not to be a similarly compelling reason why weak viscosity should alter the propagation properties as dramatically as weak confinement can.

That said, the Orr–Sommerfeld equation for viscous disturbances to a parallel (or weakly non-parallel) shear layer,

$$(U-c)(v''-\alpha^2 v)-U''v=\frac{1}{\mathrm{i}\alpha Re}(v''''-2\alpha^2 v''+\alpha^4 v), \tag{7.6}$$

i.e. the viscous extension to the Rayleigh equation, (1.2), has additional branch cuts in the complex wavenumber plane. Outside a shear layer, where $U\to U_\infty$, (7.6) reduces to

$$(U_\infty-c)(v''-\alpha^2 v)=\frac{1}{\mathrm{i}\alpha Re}(v''''-2\alpha^2 v''+\alpha^4 v), \tag{7.7}$$

which has independent solutions proportional to

$$\exp(-\sqrt{\alpha^2}y),\quad \exp(\sqrt{\alpha^2}y),\quad \exp(-\sqrt{\alpha^2+\mathrm{i}Re(\alpha U_\infty-\omega)}y), \tag{7.8a,b,c}$$

$$\exp(\sqrt{\alpha^2+\mathrm{i}Re(\alpha U_\infty-\omega)}y) \tag{7.8d}$$

of which (7.8$a$) and (7.8$c$) decay with distance from the shear layer. As noted in § 1, the square-root function in (7.8$a$), which is the inviscid solution, has a branch point at $\alpha=0$ and branch cuts on the imaginary axes of the complex wavenumber plane. The square-root function in the viscous solution, (7.8$c$), has branch points at

$$\alpha=-\frac{\mathrm{i}Re\,U_\infty}{2}\left[1\pm\left(1-\frac{4\mathrm{i}\omega}{Re\,U_\infty^2}\right)^{1/2}\right], \tag{7.9}$$

and hence for $Re\gg\omega$ at $\alpha\sim-\mathrm{i}Re\,U_\infty-\omega/U_\infty$ and $\alpha\sim\omega/U_\infty$. The branch cuts from these branch points form hyperbolae in the complex wavenmuber plane given by $\alpha_i=Re(\omega-\alpha_r U_\infty)/(2\alpha_r)$ for $|\alpha_r|$ less than its values at the branch points (7.9), where $\alpha_r=\mathrm{Re}(\alpha)$ and $\alpha_i=\mathrm{Im}(\alpha)$, and they asymptote towards the imaginary wavenumber axes as $\alpha_r\to 0$ (see Ashpis & Reshotko (1990) for sketches for a boundary-layer flow). In a mixing layer, there will also be a second set of branch points and branch cuts corresponding to the free-stream velocity in the other stream.

If the pinch point of the unconfined problem approaches these branch cuts associated with the viscous solution, then confinement, which replaces the branch cuts with infinitely many discrete modes, could destabilize the viscous problem even when it does not destabilize the inviscid problem. Future investigations might uncover such a scenario in another flow. However, the eigenvalues at the pinch point for the unconfined mixing layer shown in figure 3($a$) are $\alpha=0.1179-0.2496\mathrm{i}$ and $\omega=0.1887-0.0122\mathrm{i}$, and $U_\infty=\lim_{y\to\infty}U=1+r=2.25$ and $U_{-\infty}=\lim_{y\to-\infty}=1-r=-0.25$. This pinch point only collides with the branch cut of a viscous solution for $Re=-0.2698$, i.e. for an unphysical Reynolds number. In fact, the pinch point only collides with a branch cut of the viscous solution at $Re>0$ for $r<0.84$, i.e. when the pinch point has crossed into the left half-plane, so for this flow destabilization by confinement is only produced by the branch cuts due to the inviscid solution.

## Appendix A. Neutral waves as $\alpha\to 0$ for nearly symmetric confinement

Substituting (2.5) into (2.3) gives

$$0=\int_{-h_s-\delta}^{h_s+h_{11}\delta+h_{12}\delta^2} g(t)\,\mathrm{d}t-\frac{2h_s+(1+h_{11})\delta+h_{12}\delta^2}{(h_s+\delta)(h_s+h_{11}\delta+h_{12}\delta^2)f'(0)^2}$$

$$= \int_{-h_s-\delta}^{-h_s} g(t)\,\mathrm{d}t + \int_{-h_s}^{h_s} g(t)\,\mathrm{d}t + \int_{h_s}^{h_s+h_{11}\delta+h_{12}\delta^2} g(t)\,\mathrm{d}t$$
$$- \frac{2h_s + (1+h_{11})\delta + h_{12}\delta^2}{(h_s+\delta)(h_s+h_{11}\delta+h_{12}\delta^2)f'(0)^2}$$
$$\sim g(h_s)\delta + \frac{g'(h_s)}{2}\delta^2 + \int_{-h_s}^{h_s} g(t)\,\mathrm{d}t + g(h_s)(h_{11}\delta+h_{12}\delta^2) + \frac{g'(h_s)}{2}(h_{11}\delta+h_{12}\delta^2)^2$$
$$- \frac{1}{h_s^3 f'(0)^2}\left[2h_s^2 - h_s(1+h_{11})\delta + \left(1+h_{11}^2 - h_s h_{12}\right)\delta^2\right] + \cdots$$
$$\sim \int_{-h_s}^{h_s} g(t)\,\mathrm{d}t - \frac{2}{h_s f'(0)^2} + \frac{(1+h_{11})\left(1+f'(0)^2 g(h_s)h_s^2\right)}{f'(0)^2 h_s^2}\delta$$
$$+ \frac{\left(1+h_{11}^2\right)\left(-2+f'(0)^2 g'(h_s)h_s^3\right) + 2h_s\left(1+f'(0)^2 g(h_s)h_s^2\right)h_{12}}{2f'(0)^2 h_s^3}\delta^2 + \cdots, \quad \text{(A 1)}$$

where

$$g(t) = \frac{1}{f(t)^2} - \frac{1}{f'(0)^2 t^2}, \quad \text{(A 2)}$$

and use has been made of the fact that $g$ is an even function because $f$ is an odd function, and also that

$$\int_a^{a+b} g(t)\,\mathrm{d}t = \int_a^{a+b} g(a) + g'(a)(t-a) + \frac{g''(a)}{2}(t-a)^2 + \cdots\,\mathrm{d}t$$
$$= g(a)b + \frac{g'(a)}{2}b^2 + \frac{g''(a)}{6}b^3 + \cdots, \quad \text{(A 3)}$$

when $b$ is small. The leading-order terms of (A 1) are satisfied by (2.4). Equating the $O(\delta)$ terms to zero gives $h_{11} = -1$, and then equating the $O(\delta^2)$ terms to zero gives $h_{12} = 2f'(h_s)/f(h_s)$ by (A 2). Substituting these values into (2.5*b*) gives (2.6).

## Appendix B. Long-wave dispersion relation for asymmetric confinement

A slow spatial variable is introduced to describe the dependence of the solution in the upper and lower layers outside the mixing layer: $y = Y/\epsilon$, where $Y = O(1)$ at distances of order of wavelengths from the mixing layer. The subscripts '*u*', '*m*' and '*l*' will be used to denote variables in the upper layer, mixing layer and lower layer, respectively. The upper-layer variables at leading order are

$$u(y) = \epsilon u_{u0}(Y) + \cdots, \quad v(y) = \epsilon v_{u0}(Y) + \cdots, \quad p(y) = \epsilon p_{u0}(Y) + \cdots, \quad \text{(B 1}a, b, c\text{)}$$

and the boundary condition for the upper layer (4.4*a*) becomes $v_{u0}(h_1) = 0$ (these variables are all of the same order of magnitude so that pressure and velocity fields are coupled, and matching to the mixing layer leads to the conclusion that the upper-layer horizontal velocity component is $O(\epsilon)$ smaller than in the mixing layer). Substituting (B 1), (4.3) and $f(y) = 1$ into (4.2), equating leading-order powers of $\epsilon$ and solving using the upper-layer boundary condition gives

$$v_{u0} = A_{u0}\sinh[\alpha_0(Y-h_1)], \quad p_{u0} = -\mathrm{i}A_{u0}(1+r-c_0)\cosh[\alpha_0(Y-h_1)], \quad \text{(B 2}a, b\text{)}$$

where $A_{u0}$ is an arbitrary constant.

The leading-order mixing-layer variables are

$$u(y) = u_{m0}(y) + \cdots, \quad v(y) = \epsilon v_{m0}(y) + \cdots, \quad p(y) = \epsilon p_{m0}(y) + \cdots, \quad \text{(B 3}a, b, c\text{)}$$

where the order of magnitude of $v$ and $p$ is fixed by the requirement to match the upper-layer variables (B 1), and the order of magnitude of $u$ then follows from requiring $u$ to appear at leading order in the continuity equation (4.2$a$). Substituting (B 3) and (4.3) into (4.2), equating leading order powers of $\epsilon$ and solving gives

$$v_{m0} = A_{m0}(1 + rf(y) - c_0), \quad p_{m0} = P_{m0}, \tag{B 4$a$, $b$}$$

where $A_{m0}$ and $P_{m0}$ are arbitrary constants.

The lower-layer variables follow the same scalings as the upper-layer variables (B 1)

$$u(y) = \epsilon u_{l0}(Y) + \cdots, \quad v(y) = \epsilon v_{l0}(Y) + \cdots, \quad p(y) = \epsilon p_{l0}(Y) + \cdots, \tag{B 5$a$, $b$, $c$}$$

and the boundary condition for the lower layer (4.4$b$) becomes $v_{l0}(-h_2) = 0$. Substituting (B 5), (4.3) and $f(y) = -1$ into (4.2), equating leading-order powers of $\epsilon$ and solving using the lower-layer boundary condition gives

$$v_{l0} = A_{l0}\sinh[\alpha_0(Y + h_2)], \quad p_{l0} = -\mathrm{i}A_{l0}(1 - r - c_0)\cosh[\alpha_0(Y + h_2)], \tag{B 6$a$, $b$}$$

where $A_{l0}$ is an arbitrary constant.

Matching between the upper layer and mixing layer is achieved by letting $Y \to 0$ in (B 2), and $y \to \infty$ in (B 4) and setting the results equal to one another to give

$$-A_{u0}\sinh\alpha_0 h_1 = A_{m0}(1 + r - c_0), \quad -\mathrm{i}A_{u0}(1 + r - c_0)\cosh\alpha_0 h_1 = P_{m0}. \tag{B 7$a$, $b$}$$

Matching between the lower layer and mixing layer is achieved by letting $Y \to 0$ in (B 6), and $y \to -\infty$ in (B 4) and setting the results equal to one another to give

$$A_{l0}\sinh\alpha_0 h_2 = A_{m0}(1 - r - c_0), \quad -\mathrm{i}A_{l0}(1 - r - c_0)\cosh\alpha_0 h_2 = P_{m0}. \tag{B 8$a$, $b$}$$

Eliminating the constants $A_{u0}$, $A_{m0}$, $P_{m0}$ and $A_{l0}$ between (B 7) and (B 8) gives the leading-order long-wave dispersion relation (4.5).

## Appendix C. Long-wave dispersion relation for symmetric confinement

The derivation of the second-order long-wave theory follows closely the first-order theory summarized in Appendix B, but with boundary conditions (5.2), and we substitute the leading-order result for symmetric confinement, $c_0 = 1 + r\mathrm{i}$, directly into (5.1). The upper-layer variables are now

$$u(y) = \epsilon u_{u0}(Y) + \epsilon^2 u_{u1}(Y) + \cdots, \quad v(y) = \epsilon v_{u0}(Y) + \epsilon^2 v_{u1}(Y) + \cdots, \tag{C 1$a$, $b$}$$

$$p(y) = \epsilon p_{u0}(Y) + \epsilon^2 p_{u1}(Y) + \cdots. \tag{C 1$c$}$$

Substituting (C 1), (5.1) and $f = 1$ into (4.2), equating coefficients of powers of $\epsilon$ and solving the resulting differential equations with the boundary conditions gives

$$v_{u0} = A_{u0}\sinh[\alpha_0(Y - h_0)], \quad p_{u0} = -(1 + \mathrm{i})rA_{u0}\cosh[\alpha_0(Y - h_0)], \tag{C 2$a$, $b$}$$

$$v_{u1} = A_{u1}\sinh[\alpha_0(Y - h_0)], \quad p_{u1} = [\mathrm{i}A_{u0}c_1 - (1 + \mathrm{i})rA_{u1}]\cosh[\alpha_0(Y - h_0)], \tag{C 2$c$, $d$}$$

where $A_{u1}$ is an arbitrary constant.

The main-layer variables are

$$u(y) = u_{m0}(y) + \epsilon u_{m1}(y) + \cdots, \quad v(y) = \epsilon v_{m0}(y) + \epsilon^2 v_{m1}(y) + \cdots, \tag{C 3$a$, $b$}$$

$$p(y) = \epsilon p_{m0}(y) + \epsilon^2 p_{m1}(y) + \cdots. \tag{C 3$c$}$$

Substituting (C 3) and (5.1) into (4.2), equating coefficients of powers of $\epsilon$ and solving the resulting differential equations gives

$$v_{m0} = rA_{m0}[f(y) - \mathrm{i}], \quad p_{m0} = P_{m0}, \tag{C 4$a$, $b$}$$

$$v_{m1} = -A_{m0}c_1 + r[f(y) - \mathrm{i}]\left\{A_{m1} + \frac{\mathrm{i}\alpha_0 P_{m0}}{r^2}\int_{-a}^{y}\frac{1}{[f(t)-\mathrm{i}]^2} + \frac{\mathrm{i}}{2}\,\mathrm{d}t - \frac{\mathrm{i}}{2}y\right\}, \quad (\mathrm{C}\,4c)$$

$$p_{m1} = P_{m1} - \mathrm{i}\alpha_0 r^2 A_{m0}\left\{\int_{-a}^{y}[f(t)-\mathrm{i}]^2 - 2\mathrm{i}\,\mathrm{d}t + 2\mathrm{i}y\right\}, \quad (\mathrm{C}\,4d)$$

where $A_{m1}$ and $P_{m1}$ are arbitrary constants and $a$ is a large positive parameter; after matching, we will take $a \to \infty$. Constant terms have been included in the integrals to cause the integrands to tend to zero as $y \to -\infty$.

The lower-layer variables are

$$u(y) = \epsilon u_{l0}(Y) + \epsilon^2 u_{l1}(Y) + \cdots, \quad v(y) = \epsilon v_{l0}(Y) + \epsilon^2 v_{l1}(Y) + \cdots, \quad (\mathrm{C}\,5a, b)$$

$$p(y) = \epsilon p_{l0}(Y) + \epsilon^2 p_{l1}(Y) + \cdots. \quad (\mathrm{C}\,5c)$$

Substituting (C 5), (5.1) and $f = -1$ into (4.2), equating coefficients of powers of $\epsilon$ and solving the resulting differential equations with the boundary conditions gives

$$v_{l0} = A_{l0}\sinh[\alpha_0(Y + h_0)], \quad p_{l0} = -(1-\mathrm{i})rA_{l0}\cosh[\alpha_0(Y+h_0)], \quad (\mathrm{C}\,6a, b)$$

$$v_{l1} = A_{l1}\sinh[\alpha_0(Y + h_0)], \quad p_{l1} = [\mathrm{i}A_{l0}c_1 - (1-\mathrm{i})rA_{l1}]\cosh[\alpha_0(Y+h_0)], \quad (\mathrm{C}\,6c, d)$$

where $A_{l1}$ is an arbitrary constant.

At leading order, the solutions in each layer approach constants as they are followed into adjacent layers, which allowed a particularly simple matching procedure to be used, but at second order there is algebraic growth of the main-layer solutions as they are followed into the upper and lower layers. We use van Dyke's matching rule in this case. Solutions in each layer are written in terms of the variables that apply to the layer that they are to be matched to. The solutions are then expanded for small $\epsilon$

$$v \sim \epsilon v_{u0}(\epsilon y) + \epsilon^2 v_{u1}(\epsilon y) \sim -\epsilon\sinh(\alpha_0 h_0)A_{u0} + \epsilon^2\alpha_0\cosh(\alpha_0 h_0)A_{u0}y - \epsilon^2\sinh(\alpha_0 h_0)A_{u1} + \cdots \quad (\mathrm{C}\,7a)$$

$$p \sim \epsilon p_{u0}(\epsilon y) + \epsilon^2 p_{u1}(\epsilon y) \sim -\epsilon(1+\mathrm{i})r\cosh(\alpha_0 h_0)A_{u0} + \epsilon^2(1+\mathrm{i}) \times \alpha_0 r\sinh(\alpha_0 h_0)A_{u0}y + \epsilon^2[\mathrm{i}c_1 A_{u0} - (1+\mathrm{i})rA_{u1}]\cosh(\alpha_0 h_0) + \cdots \quad (\mathrm{C}\,7b)$$

$$v \sim \epsilon v_{m0}(Y/\epsilon) + \epsilon^2 v_{m1}(Y/\epsilon) \sim \epsilon(1-\mathrm{i})rA_{m0} - \epsilon^2 c_1 A_{m0} + \epsilon^2(1-\mathrm{i})r\left(A_{m1} + \frac{\mathrm{i}\alpha_0 P_{m0}}{r^2}\left\{\int_{-a}^{a}\frac{1}{[f(t)-\mathrm{i}]^2}\,\mathrm{d}t + \frac{\mathrm{i}Y}{2\epsilon}\right\}\right) + \cdots \quad (\mathrm{C}\,7c)$$

$$p \sim \epsilon p_{m0}(Y/\epsilon) + \epsilon^2 p_{m1}(Y/\epsilon) \sim \epsilon P_{m0} + \epsilon^2 P_{m1} - \epsilon^2\mathrm{i}\alpha_0 r^2 A_{m0}\left\{\int_{-a}^{a}[f(t)-\mathrm{i}]^2\,\mathrm{d}t - 2\mathrm{i}\frac{Y}{\epsilon}\right\} + \cdots \quad (\mathrm{C}\,7d)$$

$$v \sim \epsilon v_{m0}(Y/\epsilon) + \epsilon^2 v_{m1}(Y/\epsilon) \sim -\epsilon(1+\mathrm{i})rA_{m0} - \epsilon^2 c_1 A_{m0} - \epsilon^2(1+\mathrm{i})r\left(A_{m1} + \frac{\alpha_0 P_{m0}Y}{2r^2\epsilon}\right) + \cdots \quad (\mathrm{C}\,7e)$$

$$p \sim \epsilon p_{m0}(Y/\epsilon) + \epsilon^2 p_{m1}(Y/\epsilon) \sim \epsilon P_{m0} + \epsilon^2 P_{m1} + 2\epsilon^2\alpha_0 r^2 A_{m0}\frac{Y}{\epsilon} + \cdots \quad (\mathrm{C}\,7f)$$

$$v \sim \epsilon v_{l0}(\epsilon y) + \epsilon^2 v_{l1}(\epsilon y) \sim \epsilon\sinh(\alpha_0 h_0)A_{l0} + \epsilon^2\alpha_0\cosh(\alpha_0 h_0)A_{l0}y + \epsilon^2\sinh(\alpha_0 h_0)A_{l1} + \cdots \quad (\mathrm{C}\,7g)$$

$$p \sim \epsilon p_{l0}(\epsilon y) + \epsilon^2 p_{l1}(\epsilon y) \sim -\epsilon(1-\mathrm{i})r\cosh(\alpha_0 h_0)A_{l0} - \epsilon^2(1-\mathrm{i}) \times \alpha_0 r\sinh(\alpha_0 h_0)A_{l0}y + \epsilon^2[\mathrm{i}c_1 A_{l0} - (1-\mathrm{i})rA_{l1}]\cosh(\alpha_0 h_0) + \cdots, \quad (\mathrm{C}\,7h)$$

where the main-layer solution has been expanded both for $Y>0$, (C 7$c$, $d$) and for $Y<0$, (C 7$e$, $f$), for matching to the upper and layer lowers, respectively. Matching (C 7$a$, $b$) to (C 7$c$, $d$), and (C 7$e$, $f$) to (C 7$g$, $h$), i.e. replacing $Y$ by $\epsilon y$ and then equating like powers of $\epsilon$ and $y$ gives

$$-\sinh(\alpha_0 h_0)A_{u0} = (1-\mathrm{i})r A_{m0}, \quad \alpha_0\cosh(\alpha_0 h_0)A_{u0} = -(1-\mathrm{i})\frac{\alpha_0 P_{m0}}{2r}, \tag{C 8$a$, $b$}$$

$$-\sinh(\alpha_0 h_0)A_{u1} = -c_1 A_{m0} + (1-\mathrm{i})r\left(A_{m1} + \frac{\mathrm{i}\alpha_0 P_{m0}}{r^2}\int_{-\infty}^{\infty}\frac{1}{[f(t)-\mathrm{i}]^2}\,\mathrm{d}t\right), \tag{C 8$c$}$$

$$-(1+\mathrm{i})r\cosh(\alpha_0 h_0)A_{u0} = P_{m0}, \quad (1+\mathrm{i})\alpha_0 r\sinh(\alpha_0 h_0)A_{u0} = -2\alpha_0 r^2 A_{m0}, \tag{C 8$d$, $e$}$$

$$[\mathrm{i}c_1 A_{u0} - (1+\mathrm{i})r A_{u1}]\cosh(\alpha_0 h_0) = P_{m1} - \mathrm{i}\alpha_0 r^2 A_{m0}\int_{-\infty}^{\infty}[f(t)-\mathrm{i}]^2\,\mathrm{d}t, \tag{C 8$f$}$$

$$\sinh(\alpha_0 h_0)A_{l0} = -(1+\mathrm{i})r A_{m0}, \quad \alpha_0\cosh(\alpha_0 h_0)A_{l0} = -(1+\mathrm{i})\frac{\alpha_0 P_{m0}}{2r} \tag{C 8$g$, $h$}$$

$$\sinh(\alpha_0 h_0)A_{l1} = -c_1 A_{m0} - (1+\mathrm{i})r A_{m1}, \quad -(1-\mathrm{i})r\cosh(\alpha_0 h_0)A_{l0} = P_{m0}, \tag{C 8$i$, $j$}$$

$$-(1-\mathrm{i})\alpha_0 r\sinh(\alpha_0 h_0)A_{l0} = 2\alpha_0 r^2 A_{m0}, \quad [\mathrm{i}c_1 A_{l0} - (1-\mathrm{i})r A_{l1}]\cosh(\alpha_0 h_0) = P_{m1}, \tag{C 8$k$, $l$}$$

where the limit $a\to\infty$ has been taken (the integrals are convergent if the limits are taken in this way because the integrand approaches the same constant, but with opposite sign, when $t$ is large and positive, when $t$ is large and negative). Eliminating the eight constants of integration $A_{u0}$, $A_{u1}$, $A_{m0}$, $A_{m1}$, $P_{m0}$, $P_{m1}$, $A_{l0}$ and $A_{l1}$ between the twelve equations (C 8$a$-$l$) leads to the dispersion relation (5.3).

## Appendix D. Long-wave dispersion relation for semiconfinement

This case is quickly adapted from the solutions in Appendix B. The boundary condition (6.1$a$) becomes $v_{u0}(h_0)=0$ in the upper layer, so the upper-layer solutions (B 2) become

$$v_{u0} = A_{u0}\sinh[\alpha_0(Y-h_0)], \quad p_{u0} = -\mathrm{i}A_{u0}(1+r-c_0)\cosh[\alpha_0(Y-h_0)]. \tag{D 1$a$, $b$}$$

The mixing-layer solutions (B 4) are unaffected. The lower-layer solutions that satisfy (6.1$b$), and so decay exponentially with distance below the mixing layer, are

$$v_{l0} = A_{l0}\exp(\alpha_0 Y), \quad p_{l0} = -\mathrm{i}A_{l0}(1-r-c_0)\exp(\alpha_0 Y). \tag{D 2$a$, $b$}$$

Using the same matching procedure as in Appendix B, but applied to the solutions (D 1$a$, $b$), (B 4) and (D 2$a$, $b$), and eliminating the constants of integration gives the leading-order dispersion relation for semiconfinement, (6.2).

Note that (6.2) can also be obtained from (4.5) in the limit where $\mathrm{Re}(\alpha_0)h_2 \gg 1$ since then $\sinh[\alpha_0(h_1+h_2)]/\sinh[\alpha_0(h_2-h_1)] \sim \exp(2\alpha_0 h_1)$, which leads to (6.2) on taking $h_1 = h_0$.

## REFERENCES


Ashpis, D. E. & Reshotko, E. 1990 The vibrating ribbon problem revisited. *J. Fluid Mech.* **213**, 531–547.

Briggs, R. J. 1964 *Electron-Stream Interaction with Plasmas.* MIT.

Drazin, P. G. & Reid, W. H. 1981 *Hydrodynamic Stability Theory.* CUP.

Gaster, M. 1968 Growth of disturbances in both space and time. *Phys. Fluids* **11**, 723–727.

Healey, J. J. 2006a Inviscid long-wave theory for the absolute instability of the rotating disk-boundary layer. *Proc. R. Soc. Lond.* A **462**, 1467–1492.

Healey, J. J. 2006b A new type of convective instability with exponential growth perpendicular to the basic flow. *J. Fluid Mech.* **560**, 279–310.

Healey, J. J. 2007 Enhancing the absolute instability of a boundary layer by adding a far away plate. *J. Fluid Mech.* **579**, 29–61.

Healey, J. J. 2008 Inviscid axisymmetric absolute instability of swirling jets. *J. Fluid Mech.* **613**, 1–33.

Huerre, P. & Monkewitz, P. A. 1985 Absolute and convective instabilities in free shear layers. *J. Fluid Mech.* **159**, 151–168.

Juniper, M. P. 2006 The effect of confinement on the stability of two-dimensional shear flows. *J. Fluid Mech.* **565**, 171–195.

Juniper, M. P. 2007 The full-impulse response of two-dimensional jet/wake flows and implications for confinement. *J. Fluid Mech.* **590**, 163–185.

Juniper, M. P. & Candel, S. M. 2003 The stability of ducted compound flows and consequences for the geometry of coaxial injectors. *J. Fluid Mech.* **482**, 257–269.

Koch, W. 1985 Local instability characteristics and frequency determination of self-excited wake flows. *J. Sound and Vib.* **99**, 53–83.

Lim, D. & Redekopp, L. 1998 Absolute instability conditions for variable density, swirling jet flows. *Eur. J. Mech.* B/*Fluids* **17**, 165–185.

Michalke, A. 1964 On the inviscid instability of the hyperbolic-tangent velocity profile. *J. Fluid Mech.* **19**, 543–556.

Rayleigh, Lord 1894 *The Theory of Sound,* 2nd ed. MacMillan.

Yu, M.-H. & Monkewitz, P. A. 1990 The effect of nonuniform density on the absolute instability of two-dimensional inertial jets and wakes. *Phys. Fluids* A **2**, 1175–1181.